JCTC Journal of Chemical Theory and Computation

Article

pubs.acs.org/JCTC

Calculating X-ray Absorption Spectra of Open-Shell Molecules with the Unrestricted Algebraic-Diagrammatic Construction Scheme for the Polarization Propagator

Jan Wenzel,* Michael Wormit, and Andreas Dreuw*

Interdisciplinary Center for Scientific Computing, University of Heidelberg, Im Neuenheimer Feld 368, 69120 Heidelberg, Germany

ABSTRACT: X-ray absorption spectroscopy (XAS) is a powerful tool that provides information about the electronic structure of molecules via excitation of electrons from the K-shell core region to the unoccupied molecular levels. These high-lying electronic core-excited states can be accurately calculated using the algebraic-diagrammatic construction scheme of second order ADC(2) by applying the core−valence separation (CVS) approximation to the ADC(2) working equations. For the first time, an efficient implementation of an unrestricted CVS-ADC(2) variant CVS-UADC(2) is presented for the calculation of open-shell molecules by treating α and β spins separately from each other. The potential of the CVS-UADC(2) method is demonstrated with a set of small organic radicals by comparison with standard TD-DFT/B3LYP values and experimental data. It turns out that the extended variant CVS-UADC(2)-x, in particular, provides the most accurate results with errors of only 0.1% compared to experimental values. This remarkable agreement justifies the prediction of yet nonrecorded experimental XAS spectra like the one of the anthracene cation. The cation exhibits additional peaks due to the half-filled single-occupied molecular orbital, which may help to distinguish cation from the neutral species.

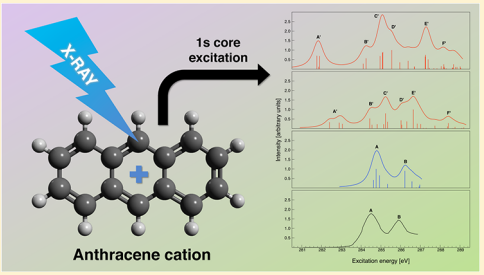

1. INTRODUCTION

X-ray absorption spectroscopy (XAS) in combination with modern synchrotron soft beam sources finds application in many fields such as organic electronics and medical biological research.[1−5] The near-edge soft X-ray absorption fine structure (NEXAFS) spectroscopy and X-ray absorption near edge structure (XANES) are widely used methods that provide, for example, information about the band structure of electrically conducting molecules to understand their conduction mechanisms.[6] Because of the strongly localized core-excited states, XAS spectra provide information about the chemical structure of a compound as well as the orientation between adsorbed molecules.[7,8] Furthermore, XAS spectroscopy helps to analyze the tautomerism of the DNA bases.[4,9,10] Since the 1s orbitals are comparatively strongly contracted, K-edge spectra are in particular element-specific and can serve as chemical fingerprints. Core excitations play also important roles in processes known as resonant intermolecular Coulombic decay (ICD), which is an efficient decay of electronically highly excited molecules in molecular environments.[11] In ICD, the core-excited molecule transfers its excess energy to a neighboring molecule, which subsequently emits a low-energy electron.[12−14] ICD processes originating from core excitations have possible applications in radiation biology, where the localized emitted electron may facilitate a more targeted cancer radiotherapy.[15,16]

Techniques in the field of time-resolved and in situ X-ray spectroscopy have been improved over the last years providing a powerful tool to explain chemical reaction mechanisms, where radicals play important roles as intermediate species, or provide information about inorganic coordination compounds.[17−19] For example, XAS techniques were able to help in analyzing the radical formation of a titanium oxide dimer or to study the electronic structure of a pyrene derivative of the nitronyl nitroxide radical.[20,21] A recent work has presented XAS spectra of the allyl radical that can help to identify key radical intermediate species in reaction mechanisms.[22] An important topic in modern applied research concentrates on materials used in organic electronics, for example, organic solar cells[23−25] or organic field-effect transistors (OFET) using organic semiconductors as the active layer.[26,27] Typical materials used in OFETs exhibit a conjugated π-electron system that provides a delocalization of the electronic wave functions in the region of the highest occupied and lowest unoccupied molecular orbitals (HOMO, LUMO), respectively. OFETs based on pentacene and its derivatives as hole conductors (p-type) have been established exhibiting large charge carrier mobilities due to its favorable crystal structure that provides excellent overlap of the frontier molecular orbitals.[28−31] X-ray absorption spectra of the pentacene cation could provide deeper insight into its charge carrier properties. However, the measurement of experimental spectra of ionized species is in general tedious.

An accurate quantum chemical description of core-excited states is thus helpful to analyze and interpret experimental spectra or to provide predictions of unmeasured molecular species. Time-dependent density functional theory (TD-DFT)[32−34] is nowadays the method of choice to describe large and medium-sized open- and closed-shell systems in

Received: July 31, 2014
Published: September 3, 2014

   dx.doi.org/10.1021/ct5006888 | J. Chem. Theory Comput. 2014, 10, 4583−4598

reasonable computational time. However, TD-DFT is hampered by the self-interaction error (SIE).[35] In conjunction with the small gap between occupied and unoccupied orbitals derived from the DFT Kohn−Sham formalism, the SIE leads to a generally strong underestimation of core-excited states.[36,37] Therefore, the excitation energies calculated at TD-DFT level usually have to be corrected by an absolute shift of several eV in energy. Furthermore, the empirical character of the exchange-correlation (xc) functionals requires an xc-functional evaluation for every molecular system of interest. An accurate and reliable benchmark method that provides precise absolute excitation energies as well as correct energy spacings is thus important. In case of closed-shell systems, various methods for the calculation of core-excited states are available. For example, the coupled cluster singles and doubles (CCSD)[38−40] method provides accurate results as well as the approximate coupled cluster scheme of second order (CC2),[41] which can be combined with a complex polarization propagator (CPP) approach to obtain core excitation spectra directly.[42] XAS spectra of open-shell systems with large multireference character can be calculated accurately with the multiconfiguration self-consistent-field (MCSCF)[22] approach.

In this work, the algebraic diagrammatic construction scheme of second order ADC(2)[43,44] for the calculation of core-excited electronic states of open-shell systems is introduced for the first time. Generally, ADC is a well-known quantum chemical method for the calculation of excited states of small and medium-sized molecules that is not hampered by SIE and thus has in contrast to TD-DFT the capability to calculate Rydberg and charge transfer states correctly.[35,45−47] Restricted ADC provides an overall accuracy for valence-excited states (UV region) of the strict version ADC(2)-s of 0.22 ± 0.5 eV, while the extended variant ADC(2)-x often underestimates the valence-excited states with an error of −0.7 ± 0.37 eV for standard organic molecules.[48] Its unrestricted variant (UADC) for valence-excited states has been introduced in 2009 and exhibits an averaged mean deviation in excitation energies for the extended variant of only 0.3−0.4 eV.[49]

Core-excited electronic states are located in the high-energy X-ray region of the spectrum. Hence, a large amount of energy is needed to excite an electron from the 1s core level to the unoccupied region. The resulting core hole leads to a strong localized spatial contraction of the electronic wave function, which can be understood as orbital relaxation. The restricted and unrestricted ADC(2) variants include an indirect description of the relaxation effects by means of the doubly excited configurations and are therefore well-suited to provide accurate excitation energies and state properties of core-excited states. Since the numerical solution of the ADC secular matrix eigenvalue problem is obtained via an iterative diagonalization procedure like the Davidson algorithm[50] yielding the energetically lowest states of the excitation spectrum, core-excited sates cannot be computed directly unless the full ADC matrix is diagonalized. However, this is computationally expensive and not feasible for larger molecules or calculations using a large number of basis functions. To solve this tedious problem elegantly, the core−valence separation (CVS) approximation is applied to the ADC working equations.[51−53] This results in a decoupling of the corresponding excitation spaces allowing for a direct diagonalization of the core excitation block.[51] Previous works are available demonstrating that CVS-ADC(2)-x yields excellent results for core-excited states of closed-shell molecules.[9,54−56] With our new implementation of restricted CVS-ADC(2) we have recently shown that the extended CVS-ADC(2)-x variant in combination with the 6-311++G** basis set exhibits errors of approximately 0.1% for core excitation energies of medium-sized molecules.[57] This excellent quantitative agreement with experimentally recorded data is due to a fortuitous compensation of errors from basis set incompleteness, orbital relaxation, relativistic effects, and electron correlation.

For the calculation of open-shell systems we have expanded our implementation[57] of CVS-ADC(2) in the adcman program[58] to the unrestricted approach CVS-UADC(2). The code is fully parallelized using unrestricted Hartree−Fock (UHF) molecular orbitals. The program exploits point group symmetry and features the calculation of excitation energies as well as oscillator strengths.

The paper is organized as follows. In Section 2 the derivation of the UADC(2) approach and the application of the CVS approximation are briefly outlined. Computational details are given in Section 3. Afterward in Section 4, first XAS spectra of radicals ever calculated with the ADC method are presented. Therefore, a set of small organic radicals was chosen to demonstrate the accuracy of the CVS-UADC(2)-x/6-311++G** approach compared to experimental data. The set consists of the methyl (CH_3), hydroxyl (OH), and allyl radicals as well as the triplet dioxygen diradical (O_2). Subsequently, the results obtained at the strict and extended CVS-UAD(2) levels of theory are compared in Section 5 with results computed using TD-DFT in combination with the B3LYP functional and with experimental values. After justifying the accuracy of the CVS-UADC(2)-x method, anthracene was chosen as a small relative of pentacene, and the XAS spectrum of the anthracene cation is predicted based on CVS-UADC(2)-x calculations in Section 6. The computed results of the anthracene cation are compared to the calculated spectrum of the neutral closed-shell species. At last, Section 7 provides a summary and concluding remarks.

2. THEORY AND IMPLEMENTATION: THE CVS APPROXIMATION APPLIED TO UADC

The derivation of the ADC formalism and the introduction of the CVS approximation has been given comprehensively in the literature.[43,44,49,51,57] In principle, the ADC working equations can be derived in two ways. Historically, the ADC scheme originates from many-body Green's function theory, where diagrammatic perturbation theory of the polarization propagator has been employed using Møller-Plesset perturbation theory[59] partitioning of the Hamiltonian. However, it is not possible to derive open-shell ADC schemes using the original pathway, because the open-shell polarization propagator is unknown. An elegant way to derive the UADC schemes is provided via the intermediate state representation (ISR) approach. Starting with the representation of the exact excited-state wave function Ψ_n in a complete basis of so-called intermediate states (IS) $|\tilde{\Psi}_I\rangle$ according to

$$\Psi_n = \sum_J X_{nJ} |\tilde{\Psi}_I\rangle \tag{1}$$

where X_{nJ} denotes eigenvectors of the ADC matrix, a matrix of the Hamiltonian shifted by the exact ground state energy E_0 is established:

$$M_{IJ} = \langle \tilde{\Psi}_I | \hat{H} - E_0 | \tilde{\Psi}_J \rangle \tag{2}$$

dx.doi.org/10.1021/ct5006888 | J. Chem. Theory Comput. 2014, 10, 4583−4598

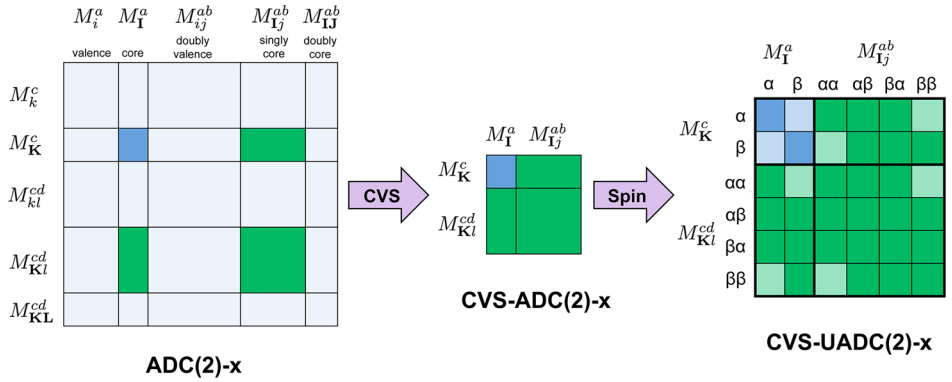

Figure 1. General illustration of the decoupling of the singly core-excited states of single and double excited configurations from the rest of the ADC(2)-x matrix by applying the CVS approximation and restriction of one index of the occupied orbitals to correspond to a core orbital resulting in a reduction of the ADC(2)-x matrix. By treating α and β spins separately the size of the resulting CVS-UADC(2)-x matrix is increased. The color of the blocks represents the order of perturbation theory (green: 1st order, blue: 2nd order). Blocks of the CVS-UADC(2)-x matrix in pale colors are zero, because transitions between α and β spin−orbitals are forbidden.

The IS $\{\tilde{\Psi}_I\}$ are constructed from a set of so-called correlated state $\{\Psi_J^0\}$ that are generated by applying an excitation operator $(\hat{C})$ to the correlated ground-state wave function Ψ_0.

$$\Psi_J^0 = \hat{C}\Psi_0 \tag{3}$$

In case of the open-shell UADC approach, $\hat{C}$ acquires spin indices leading to

$$\hat{C} \equiv \{\hat{c}_{a\sigma}^{\dagger}\hat{c}_{k\sigma};\ \hat{c}_{a\sigma}^{\dagger}\hat{c}_{b\tau}^{\dagger}\hat{c}_{k\sigma}\hat{c}_{l\tau};\ ...\} \text{ with } a\sigma < b\tau,\ k\sigma < l\tau... \tag{4}$$

which represents physical single, double, etc. excitations. These creation and annihilation operators act on spin orbitals that are either α or β orbitals. After the correlated state basis is orthonormalized via the Gram−Schmidt procedure, the resulting IS can directly be inserted into eq 2 yielding explicit expressions for the ADC matrix **M**. Thus, the hermitian eigenvalue problem

$$\mathbf{MX} = \mathbf{X\Omega},\ \mathbf{X}^{\dagger}\mathbf{X} = 1 \tag{5}$$

can now be solved to obtain the exact excitation energies $\Omega_n = E_n - E_0$ as eigenvalues. The ISR approach gives also access to transition dipole moments that can be directly obtained using

$$\mathbf{f} = \langle\tilde{\Psi}_J|\hat{\mu}|\Psi_0\rangle \tag{6}$$

where $\hat{\mu}$ represents the dipole operator.

For restricted ADC, the generally unknown exact ground state wave function is approximated via Møller−Plesset (MP) perturbation theory. Accordingly, the unrestricted Møller-Plesset (UMP) ground state is employed as reference ground state in case of UADC. Since UADC is a typical single-reference excited-state method, the scheme is sensitive to spin contamination. Therefore, the Hartree−Fock ground state reference should provide $\langle S^2\rangle$ values close to the expected number. Hence, molecules with a strong multireference character cannot be described accurately with the UADC method. Former investigations showed that $\langle S^2\rangle$ values below 1.25 for doublet radicals are still fine for UADC(2) calculations.[49] Since the α and β spins are treated separately in UADC, the dimension of the ADC matrix **M** increases compared to the restricted closed-shell implementation.

The UADC(2) matrices consist of 4 different blocks that describe the interactions of particles (p) and holes (h): p-h,p-h; p-h,2p-2h; 2p-2h,p-h; 2p-2h,2p-2h. These blocks are treated in different orders of perturbation theory. The UADC(2) method is in principle available in two variants: in the strict version UADC(2)-s the matrix elements of the 2p-2h/2p-2h block are expanded only in zeroth order, while in the extended variant UADC(2)-x they are computed in first-order perturbation theory. Explicit expressions for the matrix elements of **M** are given in the literature.[43,44] The eigenvectors of eq 5 are related to the transition amplitudes and give access to properties like transition dipole moments and oscillator strengths, respectively.

The diagonalization of the ADC matrix is typically performed using iterative diagonalization schemes like, for example, the Davidson algorithm[50] yielding the energetically lowest eigenvalues. This makes the calculation of core-excited states with the UADC method tedious, because core-excited electronic states are located in the high X-ray region of the electronic spectrum. Since valence-excited states are energetically far below the core excitations, one has to compute all excited states energetically below the core excitations. This implies a huge computational effort that makes the treatment of systems with more than 10 electrons unrealistic. A solution would be a direct diagonalization of the core-excited space, which is in general prevented by couplings between valence and core-excited states. However, the strong energetic separation of valence and core-excited states justifies the application of a core−valence separation approximation (CVS) to the UADC working equations. Since the couplings between valence and core-excited states are very small and furthermore, core orbitals are strongly localized in space and energetically well separated from the valence orbitals, these couplings can be neglected. Hence, the following types of Coulomb integrals practically vanish and can thus be set to exactly zero:

$$\begin{aligned}\langle Ip|qr\rangle = \langle pI|qr\rangle = \langle pq|Ir\rangle = \langle pq|rI\rangle = 0\\ \langle IJ|pq\rangle = \langle pq|IJ\rangle = 0\\ \langle IJ|Kp\rangle = \langle IJ|pK\rangle = \langle Ip|JK\rangle = \langle pI|JK\rangle = 0\end{aligned} \tag{7}$$

Here, capital letters *I*, *J*, *K* refer to core orbitals, and small letters *p*, *q*, *r* refer to valence orbitals. Neglecting these coupling integrals separates the singly core-excited states from the valence-excited and doubly core-excited ones. Within the implementation of the matrix-vector products for CVS-UADC, the index of the occupied orbital in the p-h configurations and one of the occupied indices in the 2p-2h configurations has to correspond to a core orbital. Therefore,

dx.doi.org/10.1021/ct5006888 | J. Chem. Theory Comput. 2014, 10, 4583−4598

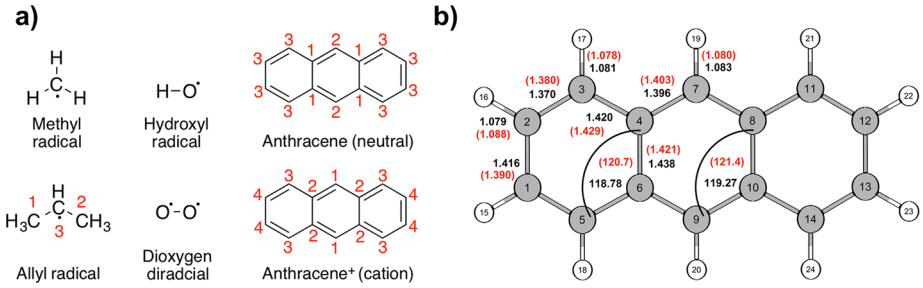

Figure 2. (a) Structures of the methyl, hydroxyl, and allyl radicals as well as the triplet dioxygen diradical and anthracene. The electron-donor orbitals that characterize the transitions are linear combinations of 1s orbitals. For a better overview, the numbering of the atoms in case of anthracene are grouped. Each group consists of similar atoms whose 1s orbitals are linearly combined into the electron donor orbitals ordered by their energy. The numbering of the atoms of the neutral and cation species differs in the amount of groups and their energetic order. (b) Comparison of the calculated structures in D_{2h} symmetry of anthracene and its cation radical (values in parentheses) at the level of RI-(U)MP2 employing the def2-TZVPP basis set. Bond distances are in [Å], and bond angles are in [deg].

only matrix elements corresponding to $M_{Ia,Kc}$ (p-h,p-h-block), $M_{Ijab,Kc}$ (2p-2h,p-h-block), $M_{Ia,Klcd}$ (p-h,2p-2h-block), and $M_{Ijab,Klcd}$ (2p-2h,2p-2h-block) need to be considered, where j and l describe occupied valence orbitals and a, b, c, and d describe virtual orbitals. Hence, the ADC matrix is substantially reduced to singly core-excited states, and direct diagonalization leads to significant computational savings compared to the conventional UADC approach (Figure 1).

CVS-UADC(2) was implemented in the adcman program[58] available in the Q-Chem program package.[60] The tensor operations required to solve the ADC eigenvalue problem are perfomed using the parallelized general-purpose tensor library libtensor.[61] It provides the infrastructure for adcman to create tensors of arbitrary rank and size, and to perform linear algebra operations on them. The library supports spin and point group symmetry, and thereby no special symmetry-adapted versions of the ADC equations are required to perform symmetry-aware calculations. The calculation of transition moments are performed using the transition density matrix, which are obtained from the spectral amplitudes derived from the ADC formalism after applying the CVS approximation.

Note that relativistic effects are not included within the general CVS-UADC approach. Core absorption spectra of light elements are not significantly influenced by relativistic effects, and the contribution is only a positive shift of the absolute energy.[53] The energy shift due to relativistic effects can be estimated to be about 0.1 eV for C 1s and 0.4 eV for O 1s excitations.[53] All computed values shown in this work are absolute without any level shift or consideration of relativistic effects.

3. COMPUTATIONAL DETAILS

Ground-state geometry optimizations were performed at the unrestricted second order Møller−Plesset perturbation theory (UMP2)[59] level employing the def2-TZVPP[62] basis set combined with the resolution-of-the-identity (RI)[63,64] approximation and the respective auxiliary TZVPP basis set.[65] The structure of neutral anthracene was optimized using the restricted second order Møller−Plesset perturbation theory (MP2)[59] in combination with the def2-TZVPP basis set, the RI approximation, and the respective auxiliary TZVPP basis set. The RI-MP2 method in combination with the def2 basis set series is known for providing accurate structures.[62,65−67] All geometry optimizations were performed using the TURBOMOLE 6.3.7 program.[68] To save computational time, the molecular point group symmetry D_{2h} was exploited in the calculations of anthracene.

The core-excited states are calculated with our implementations of CVS-UADC(2)-s and CVS-UADC(2)-x as described above. Neutral anthracene was calculated using the restricted closed-shell implementation CVS-ADC(2)-x.[57] TD-DFT calculations of the core-excited states were performed employing the B3LYP exchange-correlation functional[69−71] as implemented in the ORCA 2.8 program.[72] The calculation of K-edge XAS spectra is realized by including only excitations from the respective 1s orbitals in the TD-DFT calculations.[73,74] All core-level excitation calculations were performed using the 6-311++G**[75,76] basis set, because Pople-type basis sets, in particular the 6-311++G** due to the polarization and diffuse basis functions, have provided accurate results compared to experimental data as shown in previous work.[4,9,10,56,57] The CVS-UADC(2) and CVS-ADC(2) results are computed using the Cartesian 6D/10F version of the respective basis sets, while due to technical limitations the TD-DFT calculations are performed employing the pure 5D/7F versions. The influence of the Cartesian d and f functions on the TD-DFT results should be comparatively small, since the inherent self-interaction error is very large (up to 4% in case of C 1s excitations).[57]

The calculated spectra of anthracene are plotted by generating spectral envelopes by convoluting the discrete excited states (stick spectrum) with Lorentzians of 0.6 eV full width at half-maximum (fwhm).

4. X-RAY ABSORPTION SPECTRA OF SMALL ORGANIC RADICALS CALCULATED AT THE LEVEL OF CVS-UADC(2)-X

For the first time, the capabilities of CVS-UADC(2)-x are presented in this section by means of its application to a set of small organic radicals: at first, the methyl and hydroxyl radicals are investigated followed by the triplet dioxygen diradical and the allyl radical (see Figure 2a). The OH radical is a rife molecule in the Earth's atmosphere, where it is involved in oxidation reactions, as well as it generally participates in combustion reactions.[77,78] In the petroleum cracking industry the methyl and allyl radicals occur as precursors and intermediates, while the latter also serves as model system to study chemical dynamics of radicals.[22,79−81]

The characterization of the core-excited states is done by means of the molecular spin−orbital (sMO) configurations using the sMO expansion coefficients. An electronic excited

dx.doi.org/10.1021/ct5006888 | J. Chem. Theory Comput. 2014, 10, 4583−4598

state in terms of UADC(2) is represented by combinations of singly and doubly excited configurations; thus, there is often no single dominant configuration that is able to describe the actual excited state sufficiently. Therefore, only the main transitions with a contribution larger than 6.25% are shown. Furthermore, only pictures of relevant molecular orbitals are presented. Virtual orbitals are labeled according to their spin (α or β). For example, $\pi^*_{\alpha 1}$ denotes the lowest unoccupied orbital with α-spin, which in this case has π^* character.

4.1. Core-Excited States of the Methyl and Hydroxyl Radicals. Our CVS-ADC calculations of the methyl radical are compared to gas phase experiments, in which the CH_3 radical was generated in a supersonic molecular beam by flash pyrolysis of azomethane seeded in helium.[82] The relevant spin−orbitals are illustrated in Figure 3, and the CVS-ADC(2)-x results are

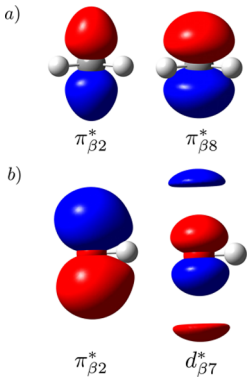

Figure 3. Illustration of the relevant virtual molecular orbitals (isovalue = 0.06) of (a) the CH_3 radical and (b) the OH radical at the level of UHF/6-311++G**.

Table 1. Excitation Energies (ω_{ex}), Oscillator Strengths (f_{osc}), Character and Amount of Double Amplitudes ($R2$) of the First Five C 1s Excited States of the CH_3 Radical Calculated Using CVS-UADC(2)-x/6-311++G[a]**

state	ω_{ex} [eV]	f_{osc}	main transition (C 1s →)	$R2$ [%]	ω_{ex} [eV] (expt.)
1	281.42	0.036	$\pi^*_{\beta 2}$, $\pi^*_{\beta 8}$	14	281.35
2	286.83	0.000	$\pi^*_{\beta 1}$, $\pi^*_{\beta 9}$	22	
3	287.72	0.000	$\pi^*_{\alpha 1}$, $\pi^*_{\alpha 8}$	23	
4	288.23	0.005	$\pi^*_{\beta 4}$, $\pi^*_{\beta 11}$	22	
5	288.23	0.005	$\pi^*_{\beta 3}$, $\pi^*_{\beta 20}$	22	

[a]The calculated values are compared with experimental data.[82] Only the main transitions are shown.

given in Table 1. The geometry optimization at the level of RI-UMP2/def2-TZVPP exhibits a planar equilibrium structure with C−H distances of r_e = 1.072 Å and an angle of α_e = 120.0°. The $\langle S^2 \rangle$ value is 0.76 at the level of UHF/6-311++G** and therefore close to the optimum value of 0.75. The experimental absorption spectrum shows a vibrational structure consisting of four peaks between 281 and 283 eV that belong to a single bright electronic transition with an excitation energy of 281.35 eV. The respective electronic excited state calculated at the level of CVS-UADC(2)-x possesses an excitation energy of 281.42 eV and therefore almost perfectly matches the experimental value. The absolute error is only 0.07 eV (0.02%), which is much smaller compared to the general error of ADC(2) for valence-excited states. This state is mostly characterized by two transitions from the carbon 1s orbital to the carbon 2p spin−orbitals with an amount of 40% for $\pi^*_{\beta 2}$ and $\pi^*_{\beta 8}$, respectively. Hence, a significant overlap with the C 1s orbital exists, resulting in an oscillator strength of 0.036. The amount of doubly excited amplitudes is 14%; thus, the state features orbital relaxation effects that are included via the double excitations. However, the amount of doubly excited amplitudes is approximately 10% smaller than the ones of closed shell systems that had been investigated in previous work[57] indicating smaller relaxation effects. The next higher core-excited states do not have oscillator strength and will therefore not be discussed here.

The experimental data for the OH radical is also obtained in gas phase, where the OH radical is produced directly with the reaction H + NO_2 → OH + NO.[83] The computed spin−orbitals are illustrated in Figure 3, and the CVS-UADC(2)-x results are given in Table 2. Note that, because of the large

Table 2. Excitation Energies (ω_{ex}), Oscillator Strengths (f_{osc}), Character and Amount of Double Amplitudes ($R2$) of the First Five O 1s Excited States of the OH Radical Calculated Using CVS-UADC(2)-x/6-311++G[a]**

state	ω_{ex} [eV]	f_{osc}	main transition (C 1s →)	$R2$ [%]	ω_{ex} [eV] (expt.)
1	525.17	0.0449	$\pi^*_{\beta 2}$, $d^*_{\beta 7}$	11	525.85
2	534.86	0.0041	$\pi^*_{\beta 1}$, $\pi^*_{\beta 5}$, $\pi^*_{\beta 3}$	19	
3	536.19	0.0115	$\pi^*_{\alpha 1}$, $\pi^*_{\alpha 3}$, $\pi^*_{\alpha 5}$	20	
4	538.81	0.0077	$\pi^*_{\beta 3}$, $\pi^*_{\beta 1}$	19	
5	539.77	0.0070	$\pi^*_{\beta 4}$	19	

[a]The calculated values are compared with experimental data.[83] Only the main transitions are shown.

polarized and diffuse 6-311++G** basis set, the orbital $d^*_{\beta 7}$ does not have a clear π^* character, because it is dominated by the diffuse functions, which correspond to weakly bound additional electrons at the UHF level. The geometry optimzation at the RI-UMP2/def2-TZVPP level results in an equilibrium O−H distance of 0.966 Å, which is in perfect agreement with experimental data (0.970 Å).[83] Similar to the methyl radical the $\langle S^2 \rangle$ value of 0.76 indicates hardly any spin contamination of the reference determinant. The experimental spectrum features a vibrationally resolved peak structure between 525 and 527.5 eV that belongs to a single bright electronic transition with the experimental value of 525.85 eV. The CVS-UADC(2)-x calculation provides a value of 525.17 eV with an absolute error of only 0.68 eV (0.1%). The amount of double excitations included in this state is 11% and therefore again much lower than for the nonradical molecules investigated in previous work.[57] The character of the first core-excited state is dominated by a transition from the oxygen 1s orbital to the O 2p-orbital with 63.1% ($\pi^*_{\beta 2}$) and 21.2% ($d^*_{\beta 7}$), respectively. The next higher calculated core-excited states also exhibit oscillator strength, but there are no experimental data available for comparison.

4.2. X-ray Absorption Spectrum of the Allyl Radical. The experiments of the allyl free radical were again performed in gas phase by flash pyrolysis of allyl iodide and 1,5-hexadiene.[22] The relevant spin−orbitals are shown in Figure 4, and the results of the CVS-UADC(2)-x calculation are summarized in Table 3. The geometry optimization at the level of RI-UMP2/def2-TZVPP provides an equilibrium C−C

dx.doi.org/10.1021/ct5006888 | J. Chem. Theory Comput. 2014, 10, 4583−4598

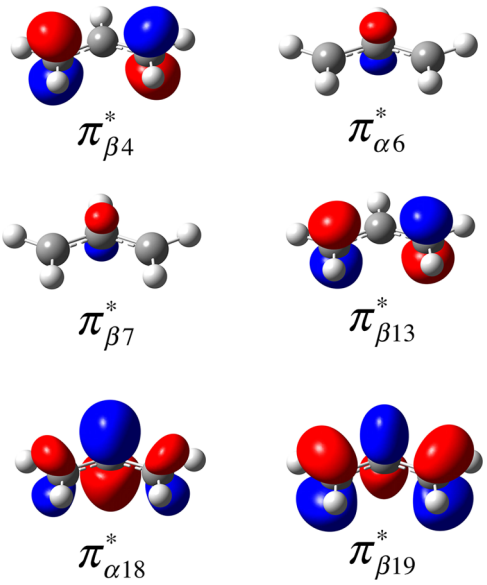

Figure 4. Illustration of the relevant virtual molecular orbitals (isovalue = 0.06) of the allyl radical at the level of UHF/6-311++G**.

bond length of 1.371 Å, which underestimates the experimental value of 1.428 Å.[84] However, the calculated CCC angle of 124.3° is in good agreement with the experiment (124.6°). The $\langle S^2 \rangle$ value of the reference determinant is 0.94 indicating small spin contamination. Since previous work reported acceptable UADC(2) results for valence excited-states of doublet radicals with $\langle S^2 \rangle$ values below 1.25, the CVS-UADC(2)-x method can be employed for the allyl radical.[49] Because of symmetry, the states 1 and 2 as well as the states 5 and 6 are almost degenerate. State 2 exhibits oscillator strength of 0.056 and is characterized by transitions from the terminal carbon 1s orbitals (linear combination) to the $\pi^*_{\beta 4}$ and $\pi^*_{\beta 13}$ spin−orbitals. These virtual orbitals are linear combinations of the empty 2p orbitals of the terminal C1/C2 atoms. The experimental excitation energy of 281.99 eV is slightly overestimated by 0.38 eV (0.1%) at the CVS-UADC(2)-x level. The amount of double configurations is also about 10%, and thus again lower compared to closed-shell molecules investigated in previous work.[57] The second bright state with the experimental value of 285.27 eV is found at a calculated energy of 284.78 eV (state 4) at the CVS-UADC(2)-x level. Here, the amount of doubly excited amplitudes is 16%, and the state is characterized by a transition from the middle carbon atom 1s orbital to delocalized π^*_α spin−orbitals. However, this state is underestimated by 0.2% leading to a poor energy gap of 2.41 eV between the two first bright states, while experimentally the difference is 3.28 eV. The third dipole-allowed transition is again underestimated by 0.6 eV leading to a relative error to the experiment of 0.2%. Hence, the energy gap between the second and third bright states is calculated to be 2.12 eV and matches the experimental one of 2.23 eV. This state is characterized by an electron promotion from the 1s orbitals located at the terminal carbon atoms to delocalized π^*_β spin−orbitals, which correspond to the π^*_α spin−orbitals of state 4 (see Figure 4). Here, the amount of double amplitudes is 27% and therefore at the typical level of the closed-shell molecules.

4.3. X-ray Absorption Spectrum of the Triplet Dioxygen Diradical. The O−O equilibrium bond length calculated at the RI-UMP2 level is 1.222 Å and is thus in excellent agreement with the experimental value[85] of 1.21 Å. The $\langle S^2 \rangle$ value is 2.05 at the level of UHF indicating hardly any spin contamination of the ground-state reference wave function. Because of the diffuse basis functions the relevant orbitals $d^*_{\alpha 1}$, $d^*_{\beta 3}$, $d^*_{\beta 7}$, $d^*_{\alpha 9}$, and $d^*_{\beta 11}$ of the triplet O_2 diradical (Figure 5) do not have a clear π^* character. The results of the

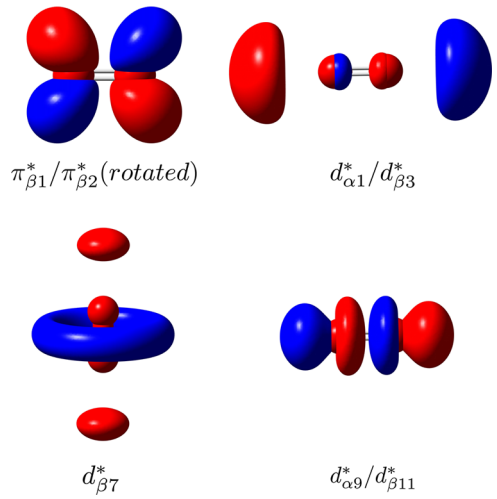

Figure 5. Illustration of the relevant virtual molecular orbitals (isovalue = 0.06) of the triplet O_2 diradical at the level of UHF/6-311++G**.

CVS-UADC(2)-x calculation are given in Table 4. The experimental spectrum exhibits three main peaks below the ionization limit with the first peak at 530.7 eV.[87,86] The CVS-UADC(2)-x calculation yields two degenerate states at an

Table 3. Excitation Energies (ω_{ex}), Oscillator Strengths (f_{osc}), Character and Amount of Double Amplitudes (R2) of the First Eight C 1s Excited States of the Allyl Radical Calculated Using CVS-UADC(2)-x/6-311++G[a]**

state	ω_{ex} [eV]	f_{osc}	main transition (C 1s →)	R2 [%]	ω_{ex} [eV] (expt.)
1	282.37	0.001	C3 → $\pi^*_{\beta 4}$, $\pi^*_{\beta 13}$	16	
2	282.37	0.056	C1,C2 → $\pi^*_{\beta 4}$, $\pi^*_{\beta 13}$	16	281.99
3	284.40	0.000	C1,C2 → $\pi^*_{\beta 4}$, $\pi^*_{\beta 13}$	29	
4	284.78	0.022	C3 → $\pi^*_{\alpha 18}$, $\pi^*_{\alpha 6}$	16	285.27
5	286.70	0.000	C3 → $\pi^*_{\beta 1}$, $\pi^*_{\beta 2}$	24	
6	286.70	0.001	C1,C2 → $\pi^*_{\beta 1}$, $\pi^*_{\beta 2}$	24	
7	286.90	0.026	C1,C2 → $\pi^*_{\beta 19}$, $\pi^*_{\beta 7}$	27	287.50
8	286.93	0.002	C3 → $\pi^*_{\alpha 1}$, $\pi^*_{\alpha 3}$	23	

[a]The calculated values are compared with experimental data.[22] Only the main transitions are shown. The numbering of the atoms complies with Figure 2a.

dx.doi.org/10.1021/ct5006888 | J. Chem. Theory Comput. 2014, 10, 4583−4598

Table 4. Excitation Energies (ω_{ex}), Oscillator Strengths (f_{osc}), Character and Amount of Double Amplitudes ($R2$) of the First 25 O 1s Excited States of the Triplet O_2 Diradical Calculated Using CVS-UADC(2)-x/6-311++G[a]**

state	ω_{ex} [eV]	f_{osc}	main transition (1s →)	$R2$ [%]	ω_{ex} [eV] (expt.)
1	529.82	0.0531	$s_{\beta 2} \rightarrow \pi^*_{\beta 2}$	21	530.7
2	529.82	0.0531	$s_{\beta 2} \rightarrow \pi^*_{\beta 1}$	21	
3	529.85	0.0000	$s_{\beta 1} \rightarrow \pi^*_{\beta 2}$	21	
4	529.85	0.0000	$s_{\beta 1} \rightarrow \pi^*_{\beta 1}$	21	
5	536.85	0.0000	$s_{\alpha 2} \rightarrow d^*_{\alpha 9}$, $d^*_{\alpha 1}$; $s_{\beta 2} \rightarrow d^*_{\beta 11}$, $d^*_{\beta 3}$	26	
6	536.87	0.0017	$s_{\alpha 1} \rightarrow d^*_{\alpha 9}$, $d^*_{\alpha 1}$; $s_{\beta 1} \rightarrow d^*_{\beta 11}$, $d^*_{\beta 3}$	26	
7	538.68	0.0000	$s_{\beta 2} \rightarrow \pi^*_{\beta 2}$, $d^*_{\beta 11}$; $s_{\alpha 2} \rightarrow d^*_{\alpha 9}$, $d^*_{\alpha 1}$	26	538.8
8	538.69	0.0706	$s_{\beta 1} \rightarrow d^*_{\beta 3}$, $d^*_{\beta 11}$; $s_{\alpha 1} \rightarrow d^*_{\alpha 9}$, $d^*_{\alpha 1}$	26	
9	539.17	0.0003	$s_{\beta 2} \rightarrow \pi^*_{\beta 4}$	24	
10	539.21	0.0000	$s_{\beta 1} \rightarrow \pi^*_{\beta 4}$	24	
11	540.27	0.0002	$s_{\alpha 2} \rightarrow \pi^*_{\alpha 2}$	27	
12	540.29	0.0000	$s_{\alpha 1} \rightarrow \pi^*_{\alpha 2}$	27	
13	540.71	0.0000	$s_{\beta 2} \rightarrow \pi^*_{\beta 5}$	24	
14	540.71	0.0000	$s_{\beta 2} \rightarrow \pi^*_{\beta 6}$	24	
15	540.75	0.0050	$s_{\beta 1} \rightarrow \pi^*_{\beta 5}$	24	
16	540.75	0.0050	$s_{\beta 1} \rightarrow \pi^*_{\beta 6}$	24	
17	541.52	0.0000	$s_{\beta 2} \rightarrow d^*_{\beta 3}$, $d^*_{\beta 11}$	26	
18	541.55	0.0185	$s_{\beta 1} \rightarrow d^*_{\beta 3}$, $d^*_{\beta 11}$	26	
19	541.78	0.0000	$s_{\alpha 2} \rightarrow \pi^*_{\alpha 4}$	27	
20	541.78	0.0000	$s_{\alpha 2} \rightarrow \pi^*_{\alpha 3}$	27	
21	541.80	0.0056	$s_{\alpha 1} \rightarrow \pi^*_{\alpha 4}$	27	
22	541.80	0.0056	$s_{\alpha 1} \rightarrow \pi^*_{\alpha 3}$	27	541.7
23	542.51	0.0000	$s_{\alpha 2} \rightarrow d^*_{\alpha 1}$, $d^*_{\alpha 9}$	27	
24	542.51	0.0209	$s_{\alpha 1} \rightarrow d^*_{\alpha 1}$, $d^*_{\alpha 9}$; $s_{\beta 2} \rightarrow d^*_{\beta 7}$	27	
25	542.60	0.0090	$s_{\beta 2} \rightarrow d^*_{\beta 7}$; $s_{\alpha 1} \rightarrow d^*_{\alpha 1}$	25	

[a]The calculated values are compared with experimental data.[86] Only the main transitions are shown. The α and β spin-orbitals s_1 refer to the positive linear combination of the two oxygen 1s orbitals, while s_2 denotes the negative linear combination.

Table 5. Comparison of Excitation Energies (ω_{ex}) and Oscillator Strengths (f_{osc}) of the First Spectroscopic Bright C 1s Excited State of the CH_3 and the O 1s Excited State of the OH Radicals as Well as of the First Three Spectroscopic Bright C 1s Excited States of the Allyl Radical and the First Five Spectroscopic Bright O 1s Excited States of the Triplet O_2 Diradical Calculated Using CVS-UADC(2)-s/x and TD-DFT/B3LYP with Experimental Values[22,82,83,86]

	B3LYP[a]		CVS-UADC(2)-s		CVS-UADC(2)-x		expt.
bright state	ω_{ex} [eV]	f_{osc}	ω_{ex} [eV]	f_{osc}	ω_{ex} [eV]	f_{osc}	ω_{ex} [eV]
			CH_3				
1	270.91	0.034	283.97	0.043	281.42	0.036	281.35
			OH				
1	511.42	0.0444	527.67	0.0497	525.17	0.0449	525.85
			allyl				
1	271.55	0.039	285.09	0.068	282.37	0.056	281.99
2	+2.91	0.011	+2.39	0.028	+2.41	0.022	+3.28
3	+4.08	0.038	+5.35	0.032	+4.52	0.026	+5.51
			O_2				
1	516.51	0.0575	533.52	0.0602	529.82	0.0531	530.7
2	516.51	0.0575	533.52	0.0602	529.82	0.0531	
3	+8.72	0.0392	+8.90	0.0383	+8.87	0.0706	+8.1
4	+11.55	0.0109	+11.02	0.0319	+11.74	0.0185	+11.0
5	+11.80	0.0783	+12.28	0.0661	+12.69	0.0209	

[a]The calculations were performed using the 6-311++G** basis set. The values of the excitation energies are given relative to the first core-excited state of the respective molecule.

energy of 529.82 eV, which is very close to the experimental value. The absolute error is 0.88 eV (0.17%). The sum of the oscillator strengths yields a value of 0.1062. The ratio of double excitations contributing to these states are considerable, with 21% indicating strong orbital relaxation effects. The calculated excited states corresponding to the other two experimental peaks at 538.8 and 541.7 eV consist of a multitude of Rydberg states; hence, only the main transitions are here discussed. State 8 with an excitation energy of 538.69 eV exhibits an oscillator strength of 0.0706 and can be assigned to the second experimental main peak. The error is only 0.11 eV (0.02%) compared to experiment. The state is mainly characterized by a mixture of transitions to the diffuse $d^*_{\beta 3}$, $d^*_{\beta 11}$, $d^*_{\alpha 9}$, and $d^*_{\alpha 1}$ orbitals indicating the characteristics of an additional weakly

dx.doi.org/10.1021/ct5006888 | J. Chem. Theory Comput. 2014, 10, 4583−4598

bound Rydberg electron. Strong orbital relaxation effects by means of the doubly excited configurations of 26% also exist. The energy gap between the degenerate states 1 and 2 and state 8 is 8.87 eV at the CVS-UADC(2)-x level and is therefore slightly overestimated by 0.77 eV compared to the experiment. The third experimental peak at 541.7 eV is again excellently matched by the CVS-UADC(2)-x calculation yielding a value of 541.55 eV (state 18) and an error of only 0.03%. Hence, the calculated energy gap of 2.86 eV between the second and third main peaks is in perfect agreement with the experimental gap of 2.9 eV. State 18 is mainly characterized by transitions to the $d^*_{\beta 3}$ and $d^*_{\beta 11}$ orbitals and exhibits a large amount of 26% double amplitudes contributing to this state. State 24 with an excitation energy of 542.51 exhibits an oscillator strength of 0.0209, but cannot be assigned properly to the experiment. Since the third experimental peak is broad, state 24 may contribute to this peak. It is characterized by transitions to the $d^*_{\alpha 1}$, $d^*_{\alpha 9}$, and $d^*_{\beta 7}$ spin−orbitals with an amount of 27% of doubly excited configurations. In summary, the triplet O_2 diradcial spectrum is almost perfectly reproduced with the CVS-UADC(2)-x method using the 6-311++G** basis set.

5. COMPARISON OF CVS-UADC(2) TO TIME-DEPENDENT DENSITY FUNCTIONAL THEORY

In this section, the results of the CVS-UADC(2) calculations are compared with TD-DFT/B3LYP data, because TD-DFT in combination with the B3LYP functional has been shown previously to yield quite accurate results for core excitation spectra and is presently used routinely for their computations.[37,57,88−90] Table 5 summarizes the results of the computed excitation energies at the different levels of theory with respect to experimental values. Starting with the results of the C 1s excited bright peak of the CH_3 radical, TD-DFT/B3LYP underestimates its excitation energy by 10.44 eV (relative error 3.9%), while CVS-UADC(2)-s overestimates this energy by 2.62 eV (0.9%). Employing CVS-UADC(2)-x is advantageous, because the absolute value is in excellent agreement with the experiment as discussed in section 4.1. The excitation energy of the first dipole-allowed transition of the OH radical is again underestimated by TD-DFT/B3LYP with 14.43 eV (2.8%), while CVS-UADC(2)-s overestimates this state by 1.82 eV (0.3%). These two bright states of the CH_3 and OH radicals exhibit an amount of doubly excited configurations at the level of CVS-UADC(2)-s with 6%, respectively. Compared to CVS-UADC(2)-x results, this is only about half of the contribution of double amplitudes indicating a too-weak consideration of orbital relaxation effects. However, the CVS-UADC(2)-s results are also close to experimental values, but CVS-UADC(2)-x provides the most accurate result.

Turning to the results of the allyl radical, TD-DFT/B3LYP underestimates the excitation energies of the bright peaks by about 4% (10.44−11.87 eV) and furthermore, the energy spacing between the bright states of the allyl radical is also falsely described. In case of the energy gap between the first and second bright state, B3LYP provides a value of 2.9 eV and for the gap between the second and third one of only 1.18 eV, while the experiment exhibits values of 3.28 and 2.23 eV, respectively. The first gap is indeed better described at the level of TD-DFT/B3LYP than at CVS-UADC(2)-x level with 2.41 eV. The gaps obtained with CVS-UADC(2)-s with values of 2.39 and 2.96 eV, respectively, are also inaccurate compared to the experiment. The energy gap between the second and third bright state is best described at the level of CVS-UADC(2)-x with a value of 2.12 eV. Thus, in summary, CVS-UADC(2)-x provides the best results for the tested methods.

At last the results of the triplet O_2 diradical are discussed. The underestimation of the excitation energies of the three bright peaks at the level of TD-DFT/B3LYP is again considerable with 14.19, 13.58, and 13.65 eV (approximately 2.6−2.7%) compared to experiment. However, by addition of an absolute, constant energy shift to the TD-DFT results, the calculated spectrum is in a good agreement with the experimental O 1s core excitation spectrum of the triplet O_2 diradical. CVS-UADC(2)-s provides absolute errors of 2.82, 3.62, and 2.84 eV (approximately 0.5%−0.7%) for the three bright peaks, respectively, and therefore by subtraction of a constant shift, the agreement with experimental data is achieved. Overall, CVS-UADC(2)-x provides the most accurate result (see section 4.3), since the absolute values as well as the energy spacing of the experiment is almost perfectly reproduced. Note that the fourth state with large oscillator strength (bright state 5, Table 5), which cannot be properly assigned to experiment, is provided by all three methods. However, the energy gap between state 4 and 5 at the level of TD-DFT/B3LYP is only 0.25 eV, while CVS-UADC(2)-x yields a larger spacing of 0.96 eV.

In summary, the results for the small organic radicals exhibit similar quality as the ones for closed-shell molecules investigated in our previous work.[57] CVS-UADC(2)-x in combination with the 6-311++G** basis set reproduces the experimental results most accurately with relative errors between −0.2 and 0.1% and accurate absolute values for the molecules investigated in this work. CVS-UADC(2)-s slightly overestimates the core-excitation energies compared to the experiments by up to 1.1%, while TD-DFT/B3LYP strongly underestimates the excitation energies of core-excited states of the investigated radicals by up to 4% compared to the experimental values. However, the relative spectra are reproduced accurately by TD-DFT/B3LYP. These general trends are identical to the ones found for closed-shell molecules investigated in our previous work. The absolute errors of the TD-DFT/B3LYP calculations are comparatively constant, but they are significantly larger compared to CVS-UADC(2)-s. Hence, it is mandatory to shift the excitation energies to simulate core-excitation spectra at the level of TD-DFT/B3LYP.

Generally, a balanced description of electron correlation in both ground and excited state is provided via the ADC formalism. One has to consider though that relativistic effects are not included neither in the CVS-UADC(2) nor in the TD-DFT approaches. Neglect of relativistic contributions seems to cancel the inherent errors of CVS-ADC(2)-x. Since CVS-UADC(2)-x includes doubly excited configurations in first order of perturbation theory, orbital relaxation effects are generally better described than at the level of CVS-UADC(2)-s, where double excitations are treated in zeroth order of perturbation theory only. The strong underestimation of core excitation energies by TD-DFT is most likely due to unbalanced SIE resulting in a much too small energy spacing between core and valence orbitals. Overall, CVS-UADC(2)-x in combination with the 6-311++G** basis set offers a fortuitous compensation of errors from basis set incompleteness, orbital relaxation, relativistic effects, and electron correlation and is thus an accurate method to compute core-excitation spectra for direct comparison with experimental data or for prediction of

Table 6. Excitation Energies (ω_{ex}), Oscillator Strengths (f_{osc}), Character and Amount of Double Amplitudes ($R2$) of the First 10 C 1s Excited Singlet States of Anthracene with B_{1u}, B_{2u}, and B_{3u} Symmetry Calculated Using CVS-ADC(2)-x/6-311++G**[a]

state	ω_{ex} [eV]	f_{osc}	main transition	$R2$ [%]	ω_{ex}[eV] (expt.)
1 $^1B_{1u}$	284.63	0.058	C2 → π_4^*	26	
2 $^1B_{1u}$	284.76	0.139	C3 → π_4^* → π_{14}^*	25	284.5 (A)
3 $^1B_{1u}$	284.93	0.092	C3 → π_4^* → π_{14}^*	26	
4 $^1B_{1u}$	285.34	0.029	C1 → π_4^*	27	
5 $^1B_{1u}$	286.21	0.125	C1 → π_{10}^*	24	285.9 (B)
6 $^1B_{1u}$	286.57	0.048	C3 → π_{10}^*	27	
7 $^1B_{1u}$	286.79	0.003	C3 → π_{10}^*	29	
1 $^1B_{2u}$	286.91	0.000	C3 → π_1^*, π_2^*	26	
1 $^1B_{3u}$	286.93	0.011	C3 → π_1^*, π_2^*	26	
2 $^1B_{2u}$	286.97	0.024	C3 → π_1^*, π_2^*, π_3^*	26	

[a]The calculated values are compared with experimental data.[92] Only the main transitions are shown. The numbering of the carbon atoms complies with Figure 2a and refers to linear combinations of the respective carbon 1s orbitals.

not-yet-recorded spectra, which is demonstrated in the current and previous work.[57]

6. PREDICTION OF THE X-RAY ABSORPTION SPECTRUM OF THE ANTHRACENE CATION

In this section, the C 1s core excitation spectrum of the anthracene cation is predicted based on CVS-UADC(2)-x calculations. Since anthracene is larger compared to the small molecules of Sections 4 and 5, note that the larger the number of constituting atoms of a molecule the higher is the density of core-excited states within a small energy region. Hence, to keep a clear view, only spectroscopically relevant bright core-excited states with their main orbital contributions are given. To save computational time, the D_{2h} point group symmetry was exploited in all calculations. Only states belonging to the irreducible representations B_{1u}, B_{2u}, and B_{3u} are optically allowed and can possess oscillator strength.

6.1. Carbon 1s Core-Excited States of Neutral Anthracene. Let us begin with a short analysis of the C 1s X-ray absorption spectrum of the neutral closed-shell anthracene molecule in gas phase. The optimized geometrical parameters are given in Figure 2b. Compared to the experimental data[91] the structure obtained at the RI-MP2 level of theory is very well-reproduced with deviations to the crystal structure not exceeding 0.005 Å. Table 6 shows the 10 lowest core-excited states of neutral anthracene exhibiting oscillator strength at the level of CVS-ADC(2)-x, and Figure 6 displays the important molecular orbitals.

The experimental spectrum of anthracene in the gas phase[92] provides two strong peaks at 284.5 eV (A) and 285.9 eV (B) that are both almost perfectly reproduced by CVS-ADC(2)-x. Peak A is a mixture of the first three calculated excited states with B_{1u} symmetry, of which the 2 $^1B_{1u}$ state with an excitation energy of 284.76 eV exhibits the largest oscillator strength. This state is characterized by transitions from the C3 1s orbitals to the π_4^* and π_{14}^* molecular orbitals. The deviation to the experiment is only 0.26 eV (0.09%). The second peak B is represented by a mixture of two B_{1u} states, of which 5 $^1B_{1u}$ with an excitation energy of 286.21 eV exhibits the largest oscillator strength of 0.125. Compared to the experiment, the error is only 0.31 eV (0.1%), and the energy spacing between the two peaks is thus almost perfectly described with 1.45 eV (experiment: 1.40 eV). Peak B is mainly characterized by transitions from the C1 1s orbitals to the π_{10}^* orbital. All presented states exhibit a large amount of doubly excited configurations >25%, which indicates strong orbital relaxation effects. Note that the experimental spectrum provides a series of Rydberg states in the energy region beyond 290 eV that will not be discussed here. In Figure 7 the calculated spectrum is plotted and directly compared with the experimental one to visualize the excellent agreement between the CVS-ADC(2)-x calculation and experiment.

6.2. Prediction of the Core-Excited States of the Anthracene Cation. Overall, the excellent results of neutral anthracene obtained using the CVS-ADC(2)-x/6-311++G** approach justifies the prediction of the C 1s X-ray absorption spectrum of the anthracene cation radical (A^+), for which no experimental data is available yet. For future comparison with experimental measurements, our analysis will be performed for two limiting cases: one using the neutral ground state geometry further denoted as A_N^+ and the other one using the equilibrium ground state structure of the anthracene cation A_C^+ to allow for geometry relaxation. The latter has also been optimized exploiting D_{2h} point group symmetry, which is justified in the literature.[94−96] The first approach is suitable for experiments with very short-lived cationic intermediates, while the second requires stable cations.

In Figure 2b the structural parameters of A^+ at the level of RI-UMP2 are given and compared with the ones of the neutral species. The calculation provides again accurate geometry parameters compared to experiment[96] with mean deviations of only 0.009 Å. The following numbering of the C atoms complies with Figure 2b. Because of the half-occupied π-orbital of A^+, bond length alternations (BLA) can be observed compared to the neutral form. r(C1−C2) and r(C4−C6) are slightly shortened, while the others are elongated. The distances between C and H are almost constant (−0.003 Å) with one exception: r(C2−H16) is elongated by 0.009 Å. Because of the unrestricted ground-state determinant, the linear combinations of the C 1s orbitals differ between the neutral restricted anthracene molecule and its cation, independent of which structure is chosen. Therefore, both A_N^+ and A_C^+ exhibit four groups of linear combinations between the C 1s orbitals, while the neutral anthracene molecule displays only three groups (see Figure 2). In both structures, the groups of orbitals are ordered according to the respective orbital energies. Furthermore, the ground state of both conformers belongs to different irreducible representations of D_{2h}: $^2B_{2g}$ for A_C^+ and $^2B_{3g}$ for A_N^+, respectively.

The shapes of the relevant spin orbitals (Figure 6) of both A_C^+ and A_N^+ are almost identical. Energetic shifts occur for higher-lying orbitals. These orbitals, which are necessary to character-

dx.doi.org/10.1021/ct5006888 | J. Chem. Theory Comput. 2014, 10, 4583−4598

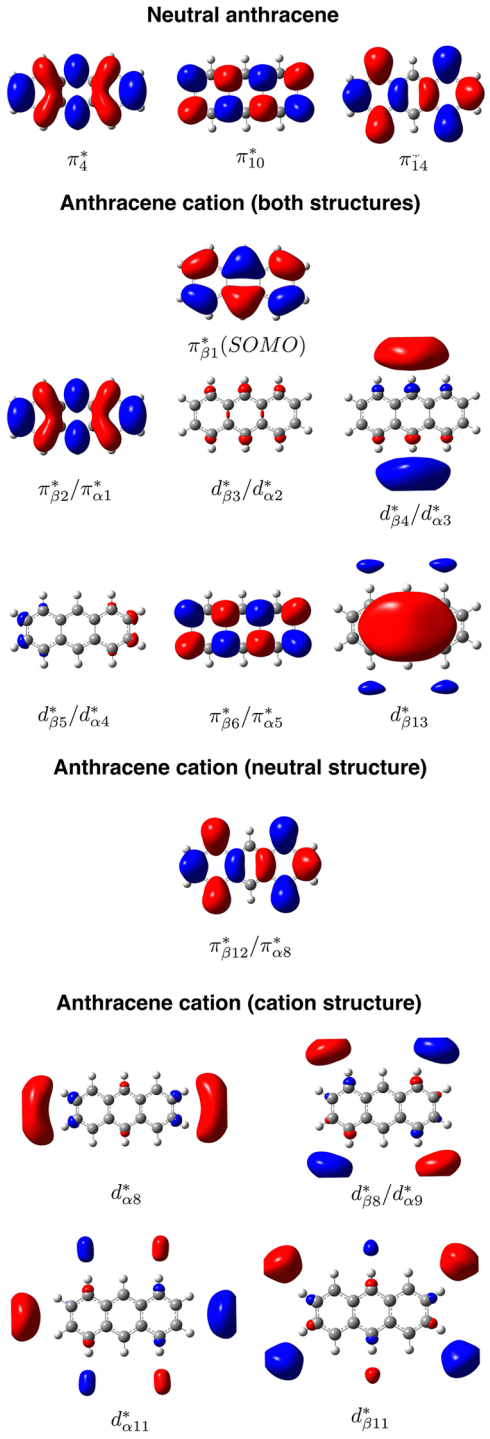

Figure 6. Illustration of the relevant virtual molecular orbitals (isovalue = 0.02) of neutral anthracene and the anthracene cation in both optimized neutral and cationic structure at the level of (U)HF/6-311++G**. Since shape and character of specific orbitals of the structures used for the cation species are identical, they are merged under "Anthracene cation (both structures)." Relevant orbitals that differ between the respective structures are given separately.

ize the bright core-excited states, are listed separately in Figure 6. Because of the BLA, the energy of the respective orbitals differs between A_C^+ and A_N^+. The singly occupied molecular orbital (SOMO, $\pi^*_{\beta1}$) is also identical in both structural conformers, but $\pi^*_{\beta1}$ of A_C^+ exhibits an energy of −0.217 au, while in A_N^+ it has a higher energy of −0.191. Due to the diffuse and polarized basis functions of the 6-311++G** basis set, extremely diffuse virtual spin orbitals occur in the low-energy regime, like $d^*_{\beta3}$ or d^*_8, which correspond to weakly bound, additional electrons at the UHF level.

The ground-state reference wave function of the A_N^+ conformer exhibits little spin contamination with $\langle S^2\rangle$ = 0.90, while $\langle S^2\rangle$ of A_C^+ is larger with 1.13. Both values are below 1.25, which has been identified as value that still provides reasonable results at the level of UADC(2)-x for doublet valence excited-states.[49]

Tables 7 and 8 summarize the results of A_N^+ and A_C^+ obtained at the CVS-UADC(2)-x level, respectively, while Figure 7 illustrates the calculated spectra simulated with a Lorentzian width of 0.6 eV fwhm. Let us start the analysis with the first bright peak assigned as A′. In the case of the A_C^+ conformer, A′ is a mixture of the first three core-excited states with B_{1u} symmetry and can be characterized by transitions from the C1, C2, and C4 groups to the SOMO. The excitation energy of 281.8 eV is about 3 eV below the first peak A of the neutral species. Because of the BLA and the higher energy of the SOMO, the A′ peak of the A_N^+ state is shifted by about 1.1 to 282.9 eV and exhibits a broader peak compared to A_C^+ with a subpeak structure leading to a shoulder with an excitation energy of 283.05 eV. Here, this state is a mixture of the first four core-excited states with B_{1u} symmetry, which still are characterized by transitions to the SOMO. In contrast to the A_C^+ conformer, an electron is also promoted from the C3 group. In both conformers due to the energetically low-lying SOMO that is filled in the neutral anthracene species, the A′ peak is well-separated from the next higher core-excited states and is therefore a characteristic attribute of the cation spectrum. Since A_C^+ and A_N^+ describe limiting cases, a very broad absorption between 281 and 283 eV can be expected in future experiments.

The next higher peak B′ can be regarded as a shoulder of the strong peak C′ and can be described as a mixture of the two next-higher core-excited states of A_C^+ and A_N^+ with almost identical excitation energies of 284.25 and 284.44 eV, respectively. Peak B′ of A_N^+ consists of transitions from C4 and C3 to the $\pi^*_{\alpha1}$ and $\pi^*_{\alpha8}$ orbitals. Both orbitals are not diffuse and have the same shape as π^*_4 and π^*_{14} of the neutral species. The same applies for C′ of A_N^+ that has the same character as B′, but with the corresponding β spin−orbitals characterizing the transitions. Therefore, B′ and C′ of A_N^+ correspond exactly to peak A of the neutral species. Since the maximum is located at C′ the excitation energy compared to A is blue-shifted by about 0.5 eV, but the absorption of the cationic species is much broader than the one of neutral anthracene. However, the characters of the transition differ between both conformers. Peak B′ of A_C^+ can be mainly described by an electron promotion from the C3 and C4 groups to the diffuse $d^*_{\alpha2}$ and $d^*_{\alpha9}$ orbitals. The strong peak C′ also includes transitions to diffuse orbitals like $d^*_{\beta11}$, $d^*_{\alpha2}$, and $d^*_{\alpha9}$, but the dominant contributions are characterized by electron promotions from the C2−C4 orbital groups to the $\pi^*_{\beta2}$ orbital, which is comparable to the one of A_N^+. However, peak C′ of A_C^+ exhibits a larger intensity than C′ of A_N^+, because the 7 B_{3u} and 8 B_{3u} states contributing to the peak are almost degenerate. Furthermore, C′ of A_C^+ exhibits an excitation energy of 285.1 eV, which is almost identical to the A_N^+ conformer.

Turning to next higher peaks D′ and E′ of A_N^+, a similar picture as for the former two peaks is provided at the level of CVS-UADC(2)-x. D′ is the shoulder of the stronger peak E′ with excitation energies of 286.0 eV (D′) and 286.6 eV (E′),

dx.doi.org/10.1021/ct5006888 | J. Chem. Theory Comput. 2014, 10, 4583−4598

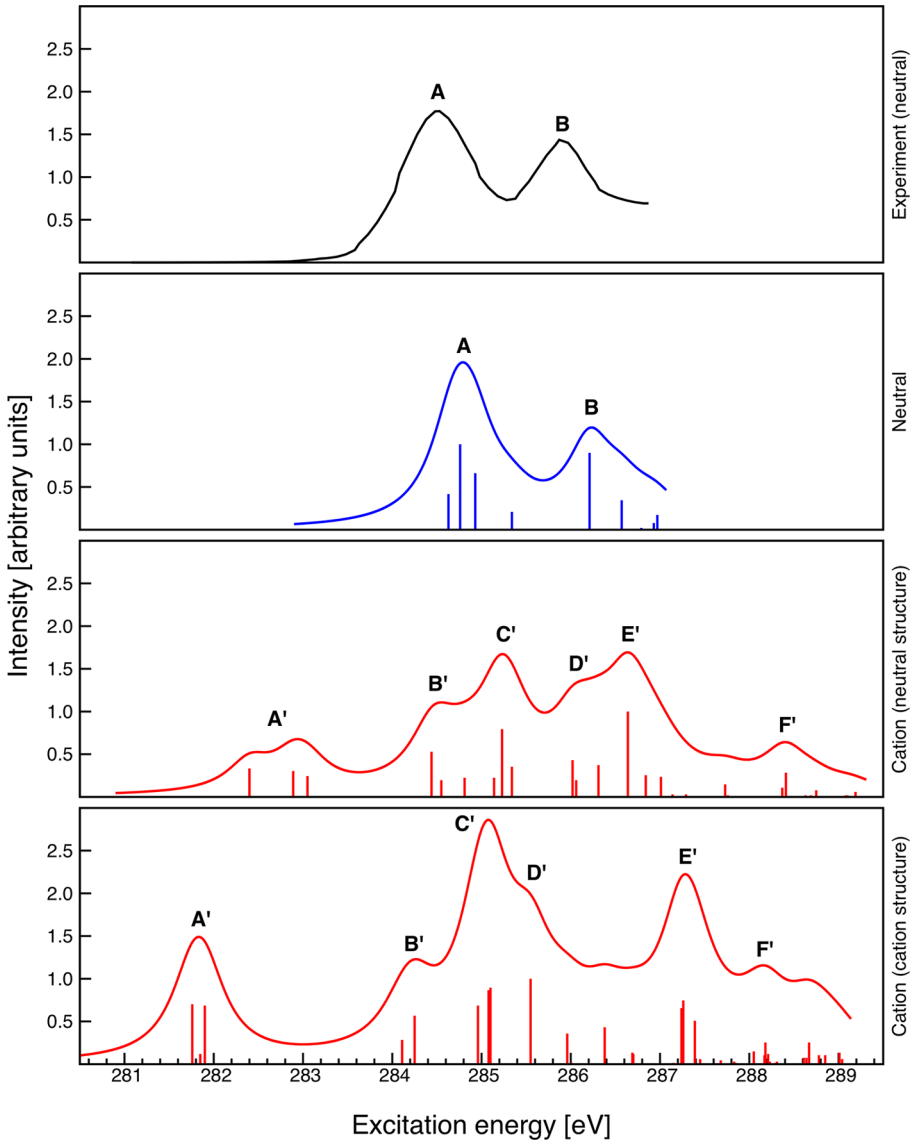

Figure 7. Comparison of X-ray absorption spectra of neutral and cationic anthracene as obtained at the CVS-(U)ADC(2)-x/6-311++G** level of theory. Furthermore, the experimental spectrum of neutral anthracene is given.[92,93] The theoretical spectra are simulated using a Lorentzian width of 0.6 eV fwhm, and all calculated excitation energies are absolute without a level shift. (upper to lower) Experimental spectrum of neutral anthracene in gas phase, neutral anthracene using the optimized neutral structure, anthracene cation using the optimized neutral structure, anthracene cation using the optimized cationic structure.

respectively. D′ is characterized by transitions from the C1 and C2 groups to the $\pi^*_{\beta 2}$, $\pi^*_{\beta 1}$, and $\pi^*_{\alpha 5}$ spin−orbitals, while the excitations corresponding to E′ are dominated by transitions to $\pi^*_{\beta 6}$, $\pi^*_{\beta 12}$, and $\pi^*_{\alpha 5}$. Since these orbitals have the same shape as the π^*_4, π^*_{10}, and π^*_{14} orbitals of the neutral species, E′ corresponds to peak B of neutral anthracene. The maximum of peak E′ located at 286.6 eV is again blue-shifted by 0.4 eV compared to B. Because of the additional absorption peak D′, peak E′ is broadened in the A^+_N conformer like it is in the case for C′ as discussed above. The intensity of C′ and E′ is almost equal, whereas for the neutral species A is distinctly larger than B. The results of the A^+_C conformer differ from those of A^+_N. Peak D′ is red-shifted by 0.47 eV and seems like a shoulder of C′ rather than E′. The transition of D′ is characterized here by electron promotion from the C2 group to the $\pi^*_{\beta 2}$, $d^*_{\beta 11}$, $\pi^*_{\beta 1}$, and $d^*_{\alpha 2}$ spin−orbitals. The character of E′ of the A^+_C conformer differs also from the one of A^+_N. Besides excitations into the $\pi^*_{\beta 2}$ orbital, the peak is dominated by transitions into diffuse orbitals. Furthermore, E′ of A^+_C is blue-shifted by 1.05 eV compared to B of the neutral species, while E′ of A^+_N exhibits a smaller shift of 0.4 eV.

Peak F′ of both A^+_N and A^+_C corresponds to higher-lying core-excited states dominated by electron promotions into a mixture of strongly diffuse orbitals. Therefore, these states correspond to Rydberg states that will not be discussed in detail in this work. F′ of A^+_N exhibits an excitation energy of 288.4 eV, while F′ of A^+_C is slightly red-shifted by 0.23 eV.

The amount of doubly excited amplitudes contributing to the excited states of both A^+_N and A^+_C is at the same level as for neutral anthracene with values between 20% and 31% indicating important contributions of orbital relaxation effects. Overall, one can expect the following features for the experimental C 1s XAS spectrum of anthracene cations compared to the neutral species: an additional broad peak due to the half-filled SOMO appears in the spectrum with excitation energies ranging from 281 to 283 eV, and for longer-

dx.doi.org/10.1021/ct5006888 | J. Chem. Theory Comput. 2014, 10, 4583−4598

Table 7. Excitation Energies (ω_{ex}), Oscillator Strengths (f_{osc}), Character and Amount of Double Amplitudes ($R2$) of the first 35 C 1s Excited States of the Anthracene Cation (Optimized Neutral Structure) with B_{1u}, B_{2u}, and B_{3u} Symmetry Calculated Using CVS-UADC(2)-x/6-311++G**[a]

state	symmetry	ω_{ex} [eV]	f_{osc}	main transition	$R2$ [%]	assignment
1 B_{2u}	B_{1u}	282.40	0.034	C1 → $\pi^*_{\beta 1}$, $\pi^*_{\beta 2}$	20	
2 B_{2u}	B_{1u}	282.89	0.031	C3 → $\pi^*_{\beta 1}$	24	A′
3 B_{2u}	B_{1u}	282.94	0.001	C2 → $\pi^*_{\beta 1}$	27	
4 B_{2u}	B_{1u}	283.05	0.025	C4 → $\pi^*_{\beta 1}$, $\pi^*_{\beta 6}$	26	
5 B_{2u}	B_{1u}	284.44	0.054	C4 → $\pi^*_{\alpha 1}$, $\pi^*_{\alpha 8}$	24	B′
6 B_{2u}	B_{1u}	284.55	0.020	C3 → $\pi^*_{\alpha 1}$, $\pi^*_{\alpha 8}$	25	
7 B_{2u}	B_{1u}	284.81	0.023	C2 → $\pi^*_{\alpha 1}$	25	
8 B_{2u}	B_{1u}	285.14	0.023	C1 → $\pi^*_{\alpha 1}$	26	
9 B_{2u}	B_{1u}	285.23	0.081	C3 → $\pi^*_{\beta 2}$, $\pi^*_{\beta 12}$	26	C′
10 B_{2u}	B_{1u}	285.34	0.036	C4 → $\pi^*_{\beta 2}$, $\pi^*_{\beta 12}$	26	
11 B_{2u}	B_{1u}	285.73	0.000	C2 → $\pi^*_{\beta 2}$, $\pi^*_{\alpha 5}$, $\pi^*_{\beta 6}$, $\pi^*_{\alpha 1}$	24	
12 B_{2u}	B_{1u}	286.02	0.044	C1 → $\pi^*_{\beta 2}$, $\pi^*_{\beta 1}$	28	D′
13 B_{2u}	B_{1u}	286.06	0.020	C2 → $\pi^*_{\beta 2}$, $\pi^*_{\alpha 5}$	27	
14 B_{2u}	B_{1u}	286.31	0.038	C4 → $\pi^*_{\alpha 2}$, $\pi^*_{\alpha 1}$, $\pi^*_{\alpha 20}$	28	
15 B_{2u}	B_{1u}	286.64	0.102	C2 → $\pi^*_{\beta 6}$, $\pi^*_{\beta 12}$, $\pi^*_{\alpha 5}$	25	E′
16 B_{2u}	B_{1u}	286.84	0.026	C3 → $\pi^*_{\alpha 8}$, $\pi^*_{\alpha 9}$, $\pi^*_{\alpha 1}$, $\pi^*_{\alpha 5}$	29	
17 B_{2u}	B_{1u}	287.01	0.024	C4 → $\pi^*_{\beta 6}$, $\pi^*_{\beta 2}$	29	
18 B_{2u}	B_{1u}	287.14	0.003	C3 → $\pi^*_{\alpha 5}$	29	
19 B_{2u}	B_{1u}	287.17	0.001	C2 → $\pi^*_{\alpha 8}$, $\pi^*_{\alpha 5}$, $\pi^*_{\alpha 9}$	28	
20 B_{2u}	B_{1u}	287.29	0.003	C3 → $\pi^*_{\beta 6}$	29	
21 B_{2u}	B_{1u}	287.54	0.001	C4 → $\pi^*_{\alpha 8}$, $\pi^*_{\alpha 9}$, $\pi^*_{\alpha 1}$	30	
22 B_{2u}	B_{1u}	287.73	0.015	C2 → $\pi^*_{\beta 12}$,$\pi^*_{\beta 6}$,$\pi^*_{\beta 9}$; C3 → $\pi^*_{\beta 2}$	28	
23 B_{2u}	B_{1u}	287.76	0.002	C2 → $\pi^*_{\beta 12}$,$\pi^*_{\beta 6}$,$\pi^*_{\beta 9}$; C3 → $\pi^*_{\beta 2}$	29	
1 B_{1u}	B_{2u}	288.07	0.001	C3 → $d^*_{\beta 3}$	25	
1 A_u	B_{3u}	288.07	0.000	C3 → $d^*_{\beta 3}$, $d^*_{\beta 4}$	25	
2 B_{1u}	B_{2u}	288.10	0.000	C4 → $d^*_{\alpha 4}$, $d^*_{\beta 5}$	25	
2 A_u	B_{3u}	288.12	0.000	C4 → $d^*_{\alpha 4}$, $d^*_{\alpha 2}$, $d^*_{\beta 5}$	25	
24 B_{2u}	B_{1u}	288.26	0.001	C4 → $\pi^*_{\beta 12}$, $\pi^*_{\beta 9}$, $\pi^*_{\beta 2}$	31	
3 B_{1u}	B_{2u}	288.34	0.000	C4 → $d^*_{\beta 3}$, $d^*_{\alpha 2}$, $d^*_{\beta 5}$, $d^*_{\alpha 4}$	26	
3 A_u	B_{3u}	288.37	0.011	C4 → $d^*_{\beta 3}$, $d^*_{\alpha 2}$, $d^*_{\beta 5}$, $d^*_{\alpha 4}$	26	
4 B_{1u}	B_{2u}	288.41	0.029	C3 → $d^*_{\alpha 2}$, $d^*_{\beta 3}$, $d^*_{\alpha 3}$	26	F′
4 A_u	B_{3u}	288.41	0.005	C3 → $d^*_{\alpha 2}$, $d^*_{\beta 3}$, $d^*_{\alpha 3}$	26	
25 B_{2u}	B_{1u}	288.63	0.002	C1 → $\pi^*_{\alpha 9}$, $\pi^*_{\alpha 15}$	32	
5 B_{1u}	B_{2u}	288.65	0.000	C2 → $d^*_{\alpha 3}$, $\pi^*_{\alpha 13}$	26	
5 A_u	B_{3u}	288.68	0.000	C2 → $d^*_{\alpha 3}$, $\pi^*_{\alpha 13}$	26	

[a]Only the main transitions are shown. The numbering of the carbon atoms complies with Figure 2a and refers to linear combinations of the respective carbon 1s orbitals. The assignment complies with Figure 7.

lived cations, one can expect a larger peak broadening due to geometry relaxation of the cation (A_C^+) compared to the neutral geometry. Our calculations may thus help in future experiments to identify anthracene cations or related species as reactive intermediates in organic materials.

7. CONCLUSION

For the first time, an implementation of strict and extended CVS-UADC(2) for the calculation of X-ray absorption spectra of open-shell molecules has been presented. The energetic and spatial separation of core and valence orbitals gives rise to the application of the core−valence separation approximation to the UADC working equations. As a consequence, the size of the ADC matrix is reduced, the core-excited states are decoupled from the valence ones, and the core-excited states can thus be computed directly and efficiently. Our implementation features excitation energies of the electronic states and properties like oscillator strengths. Furthermore, the program is parallelized and allows for the use of point group symmetry.

The capability of CVS-UADC(2) in the description of core-excited states has been demonstrated by the comparison of calculated XAS spectra at the level of CVS-UADC(2) with TD-DFT/B3LYP and experimental data for a set of small organic radicals (CH_3, OH, allyl, O_2). Similar to the results obtained using the restricted CVS-ADC(2)-x method,[57] it could be shown that very accurate results are provided by the CVS-UADC(2)-x method in combination with the 6-311++G** basis set through a fortuitous error compensation of basis set incompleteness, relativistic effects, orbital relaxation, and electron correlation. Accurate absolute excitation energies with differences of the calculated results to experimental values of only about 0.1% are archived at this level of theory. Since the ADC method like any other post-Hartree−Fock method is sensitive to the chosen basis set, a stronger overestimation must be expected for smaller basis sets. The energy spacing between

dx.doi.org/10.1021/ct5006888 | J. Chem. Theory Comput. 2014, 10, 4583−4598

Table 8. Excitation Energies (ω_{ex}), Oscillator Strengths (f_{osc}), Character and Amount of Double Amplitudes ($R2$) of the First 30 C 1s Excited States of the Anthracene Cation (Optimized Cation Structure) with B_{1u}, B_{2u}, and B_{3u} Symmetry Calculated Using CVS-UADC(2)-x/6-311++G**[a]

state	symmetry	ω_{ex} [eV]	f_{osc}	main transition	$R2$ [%]	assignment
1 B_{3u}	B_{1u}	281.76	0.047	C2 → $\pi^*_{\beta 1}$, $\pi^*_{\beta 2}$	23	
2 B_{3u}	B_{1u}	281.85	0.008	C4 → $\pi^*_{\beta 1}$; C1 → $\pi^*_{\beta 1}$	28	A′
3 B_{3u}	B_{1u}	281.90	0.046	C1 → $\pi^*_{\beta 1}$; C4 → $\pi^*_{\beta 1}$	23	
4 B_{3u}	B_{1u}	284.11	0.019	C3 → $d^*_{\alpha 2}$	20	B′
5 B_{3u}	B_{1u}	284.25	0.038	C4 → $d^*_{\alpha 2}$, $d^*_{\alpha 9}$	20	
6 B_{3u}	B_{1u}	284.96	0.046	C3 → $\pi^*_{\beta 2}$	27	
7 B_{3u}	B_{1u}	285.08	0.058	C4 → $\pi^*_{\beta 2}$, $d^*_{\beta 11}$	26	C′
8 B_{3u}	B_{1u}	285.10	0.060	C2 → $d^*_{\alpha 2}$, $d^*_{\alpha 9}$; C3 → $\pi^*_{\alpha 1}$	26	
9 B_{3u}	B_{1u}	285.55	0.067	C2 → $\pi^*_{\beta 2}$, $d^*_{\beta 11}$, $d^*_{\alpha 2}$, $\pi^*_{\beta 1}$	28	D′
10 B_{3u}	B_{1u}	285.96	0.024	C2 → $\pi^*_{\alpha 1}$; C1 → $d^*_{\alpha 2}$	24	
11 B_{3u}	B_{1u}	286.01	0.001	C4 → $\pi^*_{\alpha 1}$	28	
12 B_{3u}	B_{1u}	286.38	0.029	C1 → $\pi^*_{\beta 2}$, $d^*_{\alpha 2}$	29	
13 B_{3u}	B_{1u}	286.69	0.009	C3 → $\pi^*_{\alpha 1}$; C2 → $d^*_{\alpha 2}$	29	
14 B_{3u}	B_{1u}	286.70	0.008	C1 → $d^*_{\alpha 2}$,$\pi^*_{\beta 2}$; C2 → $\pi^*_{\alpha 1}$	29	
15 B_{3u}	B_{1u}	287.15	0.001	C4 → $d^*_{\alpha 2}$, $d^*_{\alpha 8}$, $d^*_{\alpha 9}$	28	
16 B_{3u}	B_{1u}	287.24	0.044	C4 → $\pi^*_{\beta 2}$, $d^*_{\alpha 8}$, $d^*_{\alpha 11}$	28	
17 B_{3u}	B_{1u}	287.26	0.050	C2 → $d^*_{\beta 13}$,$\pi^*_{\alpha 1}$; C1 → $d^*_{\beta 11}$	26	E′
18 B_{3u}	B_{1u}	287.39	0.034	C3 → $d^*_{\beta 13}$,$\pi^*_{\beta 40}$; C2 → $\pi^*_{\beta 2}$	27	
19 B_{3u}	B_{1u}	287.45	0.004	C3 → $d^*_{\alpha 8}$, $d^*_{\alpha 2}$, $\pi^*_{\alpha 17}$	28	
20 B_{3u}	B_{1u}	287.60	0.000	C4 → $d^*_{\beta 13}$, $\pi^*_{\beta 2}$, $\pi^*_{\beta 40}$	30	
21 B_{3u}	B_{1u}	287.68	0.003	C3 → $d^*_{\beta 8}$, $\pi^*_{\beta 2}$, $\pi^*_{\beta 16}$	30	
1 B_{1u}	B_{3u}	287.83	0.000	C4 → $d^*_{\alpha 3}$, $\pi^*_{\alpha 5}$, $d^*_{\alpha 4}$	25	
1 A_u	B_{2u}	287.83	0.002	C4 → $d^*_{\alpha 3}$, $\pi^*_{\alpha 5}$, $d^*_{\alpha 4}$	25	
2 A_u	B_{2u}	287.85	0.001	C3 → $d^*_{\alpha 3}$, $d^*_{\alpha 4}$	25	
22 B_{3u}	B_{1u}	288.01	0.000	C2 → $d^*_{\beta 11}$, $d^*_{\beta 8}$, $\pi^*_{\beta 2}$,$\pi^*_{\beta 16}$	31	
23 B_{3u}	B_{1u}	288.05	0.010	C1 → $d^*_{\alpha 9}$, $d^*_{\alpha 8}$; C2 → $\pi^*_{\alpha 1}$	29	
24 B_{3u}	B_{1u}	288.17	0.007	C2 → $d^*_{\beta 13}$; C1 → $d^*_{\beta 11}$, $d^*_{\alpha 8}$	28	F′
3 A_u	B_{2u}	288.18	0.017	C4 → $d^*_{\beta 3}$, $d^*_{\beta 5}$, $d^*_{\beta 4}$, $d^*_{\alpha 3}$	26	
2 B_{1u}	B_{3u}	288.18	0.000	C4 → $d^*_{\beta 3}$, $d^*_{\beta 5}$, $d^*_{\beta 4}$, $d^*_{\alpha 3}$	26	
4 A_u	B_{2u}	288.21	0.008	C3 → $d^*_{\beta 3}$, $d^*_{\beta 5}$, $d^*_{\alpha 3}$	26	

[a]Only the main transitions are shown. The numbering of the carbon atoms complies with Figure 2a and refer to linear combinations of the respective carbon 1s orbitals. The assignment complies with Figure 7.

the states is also well-described within the extended CVS-UADC(2) variant.

Because of the inherent self-interaction error of standard TD-DFT approaches, an almost constant underestimation of core excitation energies ranging from 2% to 4% is provided employing the B3LYP xc-functional. This is also in agreement with the results of closed-shell molecules investigated in former work.[57] Energy spacings between the states are also well-described at the level of TD-DFT/B3LYP. However, the underestimation of excitation energies clearly limits its predictive power. An experimental comparison is always mandatory for a quantitative interpretation of TD-DFT results. Keeping in mind the low computational effort of TD-DFT calculations, adequate core-absorption spectra can be obtained with TD-DFT/B3LYP by adding a large constant shift to the absolute energies.

The strict CVS-UADC(2) variant generally overestimates the excitation energies in our calculations up to 1.0% depending on the molecule. This is slightly better compared to the overestimation obtained at the restricted CVS-ADC(2)-s level, where the error is up to 1.5%.[57] Since core-excited states provide an energetically large core-hole separation, orbital relaxation effects contribute significantly to the state properties. Compared to the extended variant, the doubly excited configurations that describe the orbital relaxation effects are treated in zeroth order of perturbation theory, while CVS-ADC(2)-x also includes the first-order terms. This explains the higher accuracy provided by CVS-UADC(2)-x compared to the strict variant.

Since CVS-UADC(2)-x provides accurate absolute excitation energies and properties of core-excited states, it is well-suited to predict XAS spectra of molecules that have not been measured yet. For demonstration, the XAS spectrum of the anthracene cation has been computed. The comparison of the neutral anthracene species calculated at the level of restricted CVS-ADC(2)-x with experimental data revealed excellent agreement. It could be shown that due to the half-filled SOMO a new absorption band appears in the spectrum of the anthracene cation located approximately 3.5−1.5 eV below the first peak of neutral anthracene. Furthermore, in the cationic spectrum peak broadening can be expected for the two first peaks of neutral anthracene.

Summarizing, we have demonstrated the excellent performance of CVS-UADC(2)-x for the calculation of XAS spectra of open-shell radicals and ions that can be used as benchmark method for TD-DFT xc-functionals. In accordance with former results of closed-shell molecules,[57] the CVS-ADC(2)-x method provides very accurate results for both restricted or unrestricted

calculations. Prospective work will concentrate on a third-order implementation CVS-(U)ADC(3) providing potentially even more accurate results.

AUTHOR INFORMATION

Corresponding Authors

*E-mail: jan.wenzel@iwr.uni-heidelberg.de. (J.W.)
*E-mail: dreuw@uni-heidelberg.de. (A.D.)

Notes

The authors declare no competing financial interest.

ACKNOWLEDGMENTS

Financial funding from the Deutsche Forschungsgemeinschaft "Forschergruppe 1789 Intermolecular and Interatomic Coulombic Decay" is gratefully acknowledged. JW thanks the Heidelberg Graduate School of Mathematical and Computational Methods for the Science for their support and Tobias Setzer for using his spectrum plot package. MW acknowledges funding by the Alexander von Humboldt foundation.

REFERENCES

(1) Stöhr, J. *NEXAFS Spectroscopy;* Springer: Berlin, Germany, 1992.
(2) Urquhart, S. G.; Ade, H.; Rafailovich, M.; Sokolov, J. S.; Zhang, Y. Chemical and vibronic effects in the high-resolution near-edge X-ray absorption fine structure spectra of polystyrene isotopomers. *Chem. Phys. Lett.* **2000**, *322*, 412−418.
(3) Zubavichus, Y.; Shaporenko, A.; Grunze, M.; Zharnikov, M. Innershell Absorption Spectroscopy of Amino Acids at All Relevant Absorption Edges. *J. Phys. Chem. A* **2005**, *109*, 6998−7000.
(4) Feyer, V.; Plekan, O.; Richter, R.; Coreno, M.; de Simone, M.; Prince, K. C.; Trofimov, A. B.; Zaytseva, I. L.; Schirmer, J. Tautomerism in Cytosine and Uracil: A Theoretical and Experimental X-ray Absorption and Resonant Auger Study. *J. Phys. Chem. A* **2010**, *114*, 10270−10276.
(5) Holch, F.; Hübner, D.; Fink, R.; Schöll, A.; Umbach, E. New set-up for high-quality soft-X-ray absorption spectroscopy of large organic molecules in the gas phase. *J. Electron Spectrosc. Relat. Phenom.* **2011**, *184*, 452−456.
(6) Ikeura-Sekiguchi, H.; Sekiguchi, T. Unoccupied electronic states in polythiophene as probed by XAS and RAS. *Surf. Interface Anal.* **2008**, *40*, 673−675.
(7) Hähner, G. Near edge X-ray absorption fine structure spectroscopy as a tool to probe electronic and structural properties of thin organic films and liquids. *Chem. Soc. Rev.* **2006**, *35*, 1244−1255.
(8) Vahlberg, C.; Linares, M.; Norman, P.; Uvdal, K. Phenylboronic Ester- and Phenylboronic Acid-Terminated Alkanethiols on Gold Surfaces. *J. Phys. Chem. C* **2012**, *116*, 796−806.
(9) Plekan, O.; Feyer, V.; Richter, R.; Coreno, M.; de Simone, M.; Prince, K. C.; Trofimov, A. B.; Gromov, E. V.; Zaytseva, I. L.; Schirmer, J. A theoretical and experimental study of the near edge X-ray absorption fine structure (NEXAFS) and X-ray photoelectron spectra (XPS) of nucleobases: Thymine and adenine. *Chem. Phys.* **2008**, *347*, 360−375.
(10) Feyer, V.; Plekan, O.; Richter, R.; Coreno, M.; Vall-llosera, G.; Prince, K. C.; Trofimov, A. B.; Zaytseva, I. L.; Moskovskaya, T. E.; Gromov, E. V.; Schirmer, J. Tautomerism in Cytosine and Uracil: An Experimental and Theoretical Core Level Spectroscopic Study. *J. Phys. Chem. A* **2009**, *113*, 5736−5742.
(11) Cederbaum, L. S.; Zobeley, J.; Tarantelli, F. Giant intermolecular decay and fragmentation of clusters. *Phys. Rev. Lett.* **1997**, *79*, 4778−4781.
(12) Marburger, S.; Kugeler, O.; Hergenhahn, U.; Möller, T. Experimental Evidence for Interatomic Coulombic Decay in Ne Clusters. *Phys. Rev. Lett.* **2003**, *90*, 203401.
(13) Jahnke, T.; Sann, H.; Havermeier, T.; Kreidi, K.; Stuck, C.; Meckel, M.; Schöffler, M.; Neumann, N.; Wallauer, R.; Voss, S.; Czasch, A.; Jagutzki, O.; Malakzadeh, A.; Afaneh, F.; Weber, T.; et al. Ultrafast energy transfer between water molecules. *Nat. Phys.* **2010**, *6*, 139−142.
(14) Hergenhahn, U. Interatomic and intermolecular Coulombic decay: The early years. *J. Electron Spectrosc. Relat. Phenom.* **2011**, *184*, 78−90.
(15) Gokhberg, K.; Kolorenč, P.; Kuleff, A. I.; Cederbaum, L. S. Site- and energy-selective slow-electron production through intermolecular Coulombic decay. *Nature* **2014**, *505*, 661−663.
(16) Trinter, F.; Schöffler, M. S.; Kim, H. K.; Sturm, F. P.; Cole, K.; Neumann, N.; Vredenborg, A.; Williams, J.; Bocharova, I.; Guillemin, R.; Simon, M.; Belkacem, A.; Landers, A. L.; Weber, T.; Schmidt-Böcking, H.; et al. Resonant Auger decay driving intermolecular Coulombic decay in molecular dimers. *Nature* **2014**, *505*, 664−666.
(17) Nelson, R. C.; Miller, J. T. An introduction to X-ray absorption spectroscopy and its in situ application to organometallic compounds and homogeneous catalysts. *Catal. Sci. Technol.* **2012**, *2*, 461−470.
(18) Milne, C. J.; Penfold, T. J.; Chergui, M. Recent experimental and theoretical developments in time-resolved X-ray spectroscopies. *Coord. Chem. Rev.* **2014**, 1−25, DOI: http://dx.doi.org/10.1016/j.ccr.2014.02.013.
(19) Garino, C.; Borfecchia, E.; Gobetto, R.; van Bokhoven, J. A.; Lamberti, C. Determination of the electronic and structural configuration of coordination compounds by synchrotron-radiation techniques. *Coord. Chem. Rev.* **2014**, DOI: http://dx.doi.org/10.1016/j.ccr.2014.03.027.
(20) Mimura, N.; Tsubota, S.; Murata, K.; Bando, K. K.; Bravo-Suárez, J. J.; Haruta, M.; Oyama, S. T. Gas-phase radical generation by Ti oxide clusters supported on silica: application to the direct epoxidation of propylene to propylene oxide using molecular oxygen as an oxidant. *Catal. Lett.* **2006**, *110*, 47−51.
(21) Kakavandi, R.; Savu, S.-A.; Sorace, L.; Rovai, D.; Mannini, M.; Casu, M. B. Core-Hole Screening, Electronic Structure, and Paramagnetic Character in Thin Films of Organic Radicals Deposited on SiO 2/Si(111). *J. Phys. Chem. C* **2014**, *118*, 8044−8049.
(22) Alagia, M.; Bodo, E.; Decleva, P.; Falcinelli, S.; Ponzi, A.; Richter, R.; Stranges, S. The soft X-ray absorption spectrum of the allyl free radical. *Phys. Chem. Chem. Phys.* **2013**, *15*, 1310−1318.
(23) Lewis, N. S. Toward Cost-Effective Solar Energy Use. *Science* **2007**, *315*, 798−801.
(24) Chang, S.-Y.; Liao, H.-C.; Shao, Y.-T.; Sung, Y.-M.; Hsu, S.-H.; Ho, C.-C.; Su, W.-F.; Chen, Y.-F. Enhancing the efficiency of low bandgap conducting polymer bulk heterojunction solar cells using P3HT as a morphology control agent. *J. Mater. Chem. A* **2013**, *1*, 2447−2452.
(25) Wenzel, J.; Dreuw, A.; Burghardt, I. Charge and energy transfer in a bithiophene perylenediimide based donor-acceptor-donor system for use in organic photovoltaics. *Phys. Chem. Chem. Phys.* **2013**, *15*, 11704−11716.
(26) Dimitrakopoulos, C. D.; Malenfant, P. R. L. Organic Thin Film Transistors for Large Area Electronics. *Adv. Mater.* **2002**, *14*, 99−117.
(27) Sirringhaus, H. 25th Anniversary Article: Organic Field-Effect Transistors: The Path Beyond Amorphous Silicon. *Adv. Mater.* **2014**, *26*, 1319−1335.
(28) Lee, S.; Koo, B.; Shin, J.; Lee, E.; Park, H.; Kim, H. Effects of hydroxyl groups in polymeric dielectrics on organic transistor performance. *Appl. Phys. Lett.* **2006**, *88*, 162109.
(29) Choi, C. G.; Bae, B.-S. Effects of Hydroxyl Groups in Gate Dielectrics on the Hysteresis of Organic Thin Film Transistors. *Electrochem. Solid-State Lett.* **2007**, *10*, H347−H350.
(30) Tan, H. S.; Mathews, N.; Cahyadi, T.; Zhu, F. R.; Mhaisalkar, S. G. The effect of dielectric constant on device mobilities of high-performance, flexible organic field effect transistors. *Appl. Phys. Lett.* **2009**, *94*, 263303.
(31) Klauk, H. Organic thin-film transistors. *Chem. Soc. Rev.* **2010**, *39*, 2643−2666.
(32) Runge, E.; Gross, E. K. U. Density-functional theory for time-dependent systems. *Phys. Rev. Lett.* **1984**, *52*, 997−1000.

(33) Gross, E. K. U.; Kohn, W. Local density-functional theory of frequency-dependent linear response. *Phys. Rev. Lett.* **1985**, *55*, 2850−2852.
(34) Gross, E. K. U.; Kohn, W. Time-Dependent Density-Functional Theory. *Adv. Quantum Chem.* **1990**, *21*, 255−291.
(35) Dreuw, A.; Head-Gordon, M. Single-reference ab initio methods for the calculation of excited states of large molecules. *Chem. Rev.* **2005**, *105*, 4009−4037.
(36) Asmuruf, F. A.; Besley, N. A. Calculation of near-edge X-ray absorption fine structure with the CIS(D) method. *Chem. Phys. Lett.* **2008**, *463*, 267−271.
(37) Besley, N. A.; Asmuruf, F. A. Time-dependent density functional theory calculations of the spectroscopy of core electrons. *Phys. Chem. Chem. Phys.* **2010**, *12*, 12024−12039.
(38) Purvis, G. D., III; Bartlett, R. J. A full coupled-cluster singles and doubles model: The inclusion of disconnected triples. *J. Chem. Phys.* **1982**, *76*, 1910.
(39) Coriani, S.; Fransson, T.; Christiansen, O.; Norman, P. Asymmetric-Lanczos-Chain-Driven Implementation of Electronic Resonance Convergent Coupled-Cluster Linear Response Theory. *J. Chem. Theory Comput.* **2012**, *8*, 1616−1628.
(40) Coriani, S.; Christiansen, O.; Fransson, T.; Norman, P. Coupled-cluster response theory for near-edge x-ray-absorption fine structure of atoms and molecules. *Phys. Rev. A* **2012**, *85*, 022507.
(41) Christiansen, O.; Koch, H.; Jørgensen, P. The second-order approximate coupled cluster singles and doubles model CC2. *Chem. Phys. Lett.* **1995**, *243*, 409−418.
(42) Fransson, T.; Coriani, S.; Christiansen, O.; Norman, P. Carbon X-ray absorption spectra of fluoroethenes and acetone: A study at the coupled cluster, density functional, and static-exchange levels of theory. *J. Chem. Phys.* **2013**, *138*, 124311.
(43) Schirmer, J. Beyond the random-phase approximation: A new approximation scheme for the polarization propagator. *Phys. Rev. A* **1982**, *26*, 2395−2416.
(44) Schirmer, J.; Trofimov, A. B. Intermediate state representation approach to physical properties of electronically excited molecules. *J. Chem. Phys.* **2004**, *120*, 11449−11464.
(45) Starcke, J. H.; Wormit, M.; Schirmer, J.; Dreuw, A. How much double excitation character do the lowest excited states of linear polyenes have? *Chem. Phys.* **2006**, *329*, 39−49.
(46) Starcke, J. H.; Wormit, M.; Dreuw, A. Nature of the lowest excited states of neutral polyenyl radicals and polyene radical cations. *J. Chem. Phys.* **2009**, *131*, 144311.
(47) Harbach, P. H. P.; Dreuw, A. In *Modeling of Molecular Properties;* Comba, P., Ed.; Wiley-VCH Verlag: Weinheim, Germany, 2011; pp 29−47.
(48) Harbach, P. H. P.; Wormit, M.; Dreuw, A. The third-order algebraic diagrammatic construction method (ADC(3)) for the polarization propagator for closed-shell molecules: Efficient implementation and benchmarking. *J. Chem. Phys.* **2014**, *141*, 064113.
(49) Starcke, J. H.; Wormit, M.; Dreuw, A. Unrestricted algebraic diagrammatic construction scheme of second order for the calculation of excited states of medium-sized and large molecules. *J. Chem. Phys.* **2009**, *130*, 024104.
(50) Davidson, E. R. The iterative calculation of a few of the lowest eigenvalues and corresponding eigenvectors of large real-symmetric matrices. *J. Comput. Phys.* **1975**, *17*, 87−94.
(51) Cederbaum, L. S.; Domcke, W.; Schirmer, J. Many-body theory of core holes. *Phys. Rev. A* **1980**, *22*, 206−222.
(52) Barth, A.; Cederbaum, L. S. Many-body theory of core-valence excitations. *Phys. Rev. A* **1981**, *23*, 1038−1061.
(53) Barth, A.; Schirmer, J. Theoretical core-level excitation spectra of N2 and CO by a new polarisation propagator method. *J. Phys. B: At., Mol. Opt. Phys.* **1985**, *18*, 867−885.
(54) Trofimov, A. B.; Moskovskaya, T. E.; Gromov, E. V.; Vitkovskaya, N. M.; Schirmer, J. Core-level electronic spectra in ADC(2) approximation for polarization propagator: Carbon monoxide and nitrogen molecules. *J. Struct. Chem.* **2000**, *41*, 483−494.
(55) Trofimov, A. B.; Moskovskaya, T. E.; Gromov, E. V.; Köppel, H.; Schirmer, J. Theoretical study of K-shell excitations in formaldehyde. *Phys. Rev. A* **2001**, *64*, 022504.
(56) Bâldea, I.; Schimmelpfennig, B.; Plaschke, M.; Rothe, J.; Schirmer, J.; Trofimov, A. B.; Fanghänel, T. C 1s near edge X-ray absorption fine structure (NEXAFS) of substituted benzoic acids—A theoretical and experimental study. *J. Electron Spectrosc. Relat. Phenom.* **2007**, *154*, 109−118.
(57) Wenzel, J.; Wormit, M.; Dreuw, A. Calculating core-level excitations and x-ray absorption spectra of medium-sized closed-shell molecules with the algebraic-diagrammatic construction scheme for the polarization propagator. *J. Comput. Chem.* **2014**, *35*, 1900−1915.
(58) Wormit, M.; Rehn, D. R.; Harbach, P. H. P.; Wenzel, J.; Krauter, C. M.; Epifanovsky, E.; Dreuw, A. Investigating excited electronic states using the algebraic diagrammatic construction (ADC) approach of the polarisation propagator. *Mol. Phys.* **2014**, *112*, 774−784.
(59) Møller, C.; Plesset, M. S. Note on an approximation treatment for many-electron systems. *Phys. Rev.* **1934**, *46*, 618−622.
(60) Shao, Y.; Gan, Z.; Epifanovsky, E.; Gilbert, A. T. B.; Wormit, M.; Kussmann, J.; Lange, A. W.; Behn, A.; Deng, J.; Feng, X.; Ghosh, D.; Goldey, M.; Horn, P. R.; Jacobson, L. D.; Kaliman, I.; Khaliullin, R. Z.; Kuś, T.; Landau, A.; Liu, J.; Proynov, E. I.; Rhee, Y. M.; Richard, R. M.; Rohrdanz, M. A.; Steele, R. P.; Sundstrom, E. J.; Woodcock, H. L., III; Zimmerman, P. M.; Zuev, D.; Albrecht, B.; Alguire, E.; Austin, B.; Beran, G. J. O.; Bernard, Y. A.; Berquist, E.; Brandhorst, K.; Bravaya, K. B.; Brown, S. T.; Casanova, D.; Chang, C.-M.; Chen, Y.; Chien, S. H.; Closser, K. D.; Crittenden, D. L.; Diedenhofen, M.; DiStasio, R. J., Jr.; Do, H.; Dutoi, A. D.; Edgar, R. G.; Fatehi, S.; Fusti-Molnar, L.; Ghysels, A.; Golubeva-Zadorozhnaya, A.; Gomes, J.; Hanson-Heine, M. W. D.; Harbach, P. H. P.; Hauser, A. W.; Hohenstein, E. G.; Holden, Z. C.; Jagau, T.-C.; Ji, H.; Kaduk, B.; Khistyaev, K.; Kim, J.; Kim, J.; King, R. A.; Klunzinger, P.; Kosenkov, D.; Kowalczyk, T.; Krauter, C. M.; Lao, K. U.; Laurent, A.; Lawler, K. V.; Levchenko, S. V.; Lin, C. Y.; Liu, F.; Livshits, E.; Lochan, R. C.; Luenser, A.; Manohar, P.; Manzer, S. F.; Mao, S.-P.; Mardirossian, N.; Marenich, A. V.; Maurer, S. A.; Mayhall, N. J.; Neuscamman, E.; Oana, C. M.; Olivares-Amaya, R.; O'Neill, D. P.; Parkhill, J. A.; Perrine, T. M.; Peverati, R.; Prociuk, A.; Rehn, D. R.; Rosta, E.; Russ, N. J.; Sharada, S. M.; Sharma, S.; Small, D. W.; Sodt, A.; Stein, T.; Stück, D.; Su, Y.-C.; Thom, A. J. W.; Tsuchimochi, T.; Vanovschi, V.; Vogt, L.; Vydrov, O.; Wang, T.; Watson, M. A.; Wenzel, J.; White, A.; Williams, C. F.; Yang, J.; Yeganeh, S.; Yost, S. R.; You, Z.-Q.; Zhang, I. Y.; Zhang, X.; Zhao, Y.; Brooks, B. R.; Chan, G. K. L.; Chipman, D. M.; Cramer, C. J.; Goddard, W. A., III; Gordon, M. S.; Hehre, W. J.; Klamt, A.; Schaefer, H. F., III; Schmidt, M. W.; Sherrill, C. D.; Truhlar, D. G.; Warshel, A.; Xu, X.; Aspuru-Guzik, A.; Baer, R.; Bell, A. T.; Besley, N. A.; Chai, J.-D.; Dreuw, A.; Dunietz, B. D.; Furlani, T. R.; Gwaltney, S. R.; Hsu, C.-P.; Jung, Y.; Kong, J.; Lambrecht, D. S.; Liang, W.; Ochsenfeld, C.; Rassolov, V. A.; Slipchenko, L. V.; Subotnik, J. E.; Van Voorhis, T.; Herbert, J. M.; Krylov, A. I.; Gill, P. M. W.; Head-Gordon, M. Advances in molecular quantum chemistry contained in the Q-Chem 4 program package. *Mol. Phys.* **2014**, DOI: 10.1080/00268976.2014.952696.
(61) Epifanovsky, E.; Wormit, M.; Kuś, T.; Landau, A.; Zuev, D.; Khistyaev, K.; Manohar, P.; Kaliman, I.; Dreuw, A.; Krylov, A. I. New implementation of high-level correlated methods using a general block tensor library for high-performance electronic structure calculations. *J. Comput. Chem.* **2013**, *34*, 2293−2309.
(62) Weigend, F.; Ahlrichs, R. Balanced basis sets of split valence, triple zeta valence and quadruple zeta valence quality for H to Rn: Design and assessment of accuracy. *Phys. Chem. Chem. Phys.* **2005**, *7*, 3297−3305.
(63) Weigend, F.; Häser, M. RI-MP2: first derivatives and global consistency. *Theor. Chem. Acc.* **1997**, *97*, 331−340.
(64) Hättig, C.; Weigend, F. CC2 excitation energy calculations on large molecules using the resolution of the identity approximation. *J. Chem. Phys.* **2000**, *113*, 5154−5161.

(65) Weigend, F.; Häser, M.; Patzelt, H.; Ahlrichs, R. RI-MP2: optimized auxiliary basis sets and demonstration of efficiency. *Chem. Phys. Lett.* **1998**, *294*, 143−152.
(66) Weigend, F. Accurate Coulomb-fitting basis sets for H to Rn. *Phys. Chem. Chem. Phys.* **2006**, *8*, 1057−1065.
(67) Kossmann, S.; Neese, F. Efficient Structure Optimization with Second-Order Many-Body Perturbation Theory: The RIJCOSX-MP2Method. *J. Chem. Theory Comput.* **2010**, *6*, 2325−2338.
(68) Ahlrichs, R.; Bär, M.; Häser, M.; Horn, H.; Kölmel, C. Electronic structure calculations on workstation computers: The program system turbomole. *Chem. Phys. Lett.* **1989**, *162*, 165−169.
(69) Lee, C.; Yang, W.; Parr, R. G. Development of the Colle-Salvetti correlation-energy formula into a functional of the electron density. *Phys. Rev. B* **1988**, *37*, 785−789.
(70) Becke, A. D. Density-functional thermochemistry. III. The role of exact exchange. *J. Chem. Phys.* **1993**, *98*, 5648−5652.
(71) Becke, A. D. A new mixing of hartree-fock and local density-functional theories. *J. Chem. Phys.* **1993**, *98*, 1372−1377.
(72) Neese, F. The ORCA program system. *Wiley Interdiscip. Rev.: Comput. Mol. Sci.* **2012**, *2*, 73−78.
(73) Stener, M.; Fronzoni, G.; de Simone, M. Time dependent density functional theory of core electrons excitations. *Chem. Phys. Lett.* **2003**, *373*, 115−123.
(74) DeBeer George, S.; Petrenko, T.; Neese, F. Prediction of Iron K-Edge Absorption Spectra Using Time-Dependent Density Functional Theory †. *J. Phys. Chem. A* **2008**, *112*, 12936−12943.
(75) Krishnan, R.; Binkley, J. S.; Seeger, R.; Pople, J. A. Self-consistent molecular orbital methods. XX. A basis set for correlated wave functions. *J. Chem. Phys.* **1980**, *72*, 650.
(76) McLean, A. D.; Chandler, G. S. Contracted Gaussian basis sets for molecular calculations. I. Second row atoms, Z=11−18. *J. Chem. Phys.* **1980**, *72*, 5639.
(77) Comes, F. J. Recycling in the Earth's Atmosphere: The OH Radical—Its Importance for the Chemistry of the Atmosphere and the Determination of Its Concentration. *Angew. Chem., Int. Ed.* **1994**, *33*, 1816−1826.
(78) Hucknall, D. J. *Chemistry of hydrocarbon combustion;* Chapman Hall: London, U.K., 1985.
(79) Greensfelder, B. S.; Voge, H. H.; Good, G. M. Catalytic and Thermal Cracking of Pure Hydrocarbons: Mechanisms of Reaction. *Ind. Eng. Chem.* **1949**, *41*, 2573−2584.
(80) Leung, K. M.; Lindstedt, R. P. Detailed kinetic modeling of C1 — C3 alkane diffusion flames. *Combust. Flame* **1995**, *102*, 129−160.
(81) Fischer, I.; Chen, P. Allyl-A model system for the chemical dynamics of radicals. *J. Phys. Chem. A* **2002**, *106*, 4292−4300.
(82) Alagia, M.; Lavollée, M.; Richter, R.; Ekström, U.; Carravetta, V.; Stranges, D.; Brunetti, B.; Stranges, S. Probing the potential energy surface by high-resolution x-ray absorption spectroscopy: The umbrella motion of the core-excited CH3 free radical. *Phys. Rev. A* **2007**, *76*, 022509.
(83) Stranges, S.; Richter, R.; Alagia, M. High-resolution inner-shell photoabsorption of the OH and OD free radicals. *J. Chem. Phys.* **2002**, *116*, 3676−3680.
(84) Vajda, E.; Tremmel, J.; Rozsondai, B.; Hargittai, I.; Maltsev, A. K.; Kagramanov, N. D.; Nefedov, O. M. Molecular structure of allyl radical from electron diffraction. *J. Am. Chem. Soc.* **1986**, *108*, 4352−4353.
(85) Orville-Thomas, W. J. A bond-order/bond-length relation for oxygen-oxygen bonds. *J. Mol. Spectrosc.* **1958**, *3*, 588−591.
(86) Glans, P.; Gunnelin, K.; Skytt, P.; Guo, J. H.; Wassdahl, N.; Nordgren, J.; Ågren, H.; Gel'mukhanov, F. K.; Warwick, T.; Rotenberg, E. Resonant x-ray emission spectroscopy of molecular oxygen. *Phys. Rev. Lett.* **1996**, *76*, 2448−2451.
(87) Kosugi, N.; Shigemasa, E.; Yagishita, A. High-Resolution and Symmetry-Resolved Oxygen K-Edge Spectra of O2. *Chem. Phys. Lett.* **1992**, *190*, 481−488.
(88) Nakata, A.; Imamura, Y.; Otsuka, T.; Nakai, H. Time-dependent density functional theory calculations for core-excited states: Assessment of standard exchange-correlation functionals and development of a novel hybrid functional. *J. Chem. Phys.* **2006**, *124*, 094105.
(89) Vahlberg, C.; Linares, M.; Villaume, S.; Norman, P.; Uvdal, K. Noradrenaline and a Thiol Analogue on Gold Surfaces: An Infrared Reflection-Absorption Spectroscopy, X-ray Photoelectron Spectroscopy, and Near-Edge X-ray Absorption Fine Structure Spectroscopy Study. *J. Phys. Chem. C* **2011**, *115*, 165−175.
(90) Atkins, A. J.; Jacob, C. R.; Bauer, M. Probing the electronic structure of substituted ferrocenes with high-resolution XANES spectroscopy. *Chem.—Eur. J.* **2012**, *18*, 7021−7025.
(91) Cruickshank, D. W. J. A detailed refinement of the crystal and molecular structure of anthracene. *Acta Crystallogr.* **1956**, *9*, 915−923.
(92) Gordon, M. L.; Tulumello, D.; Cooper, G.; Hitchcock, A. P.; Glatzel, P.; Mullins, O. C.; Cramer, S. P.; Bergmann, U. Inner-Shell Excitation Spectroscopy of Fused-Ring Aromatic Molecules by Electron Energy Loss and X-ray Raman Techniques. *J. Phys. Chem. A* **2003**, *107*, 8512−8520.
(93) Hitchcock, A. P.; Mancini, D. C. Bibliography and database of inner shell excitation spectra of gas phase atoms and molecules. *J. Electron Spectrosc. Relat. Phenom.* **1994**, *67*, 1−123.
(94) Niederalt, C.; Grimme, S.; Peyerimhoff, S. D. Ab initio theoretical study of the electronic absorption spectra of polycyclic aromatic hydrocarbon radical cations of naphthalene, anthracene and phenanthrene. *Chem. Phys. Lett.* **1995**, *245*, 455−462.
(95) Hirata, S.; Lee, T. J.; Head-Gordon, M. Time-dependent density functional study on the electronic excitation energies of polycyclic aromatic hydrocarbon radical cations of naphthalene, anthracene, pyrene, and perylene. *J. Chem. Phys.* **1999**, *111*, 8904.
(96) Matsuura, A.; Nishinaga, T.; Komatsu, K. Structural Studies on the Radical Cations of Benzene, Naphthalene, Biphenylene, and Anthracene Fully Annelated with Bicyclo[2.2.2]octene Frameworks. *J. Am. Chem. Soc.* **2000**, *122*, 10007−10016.